DEVELOPMENT OF A NOVEL POLYAZAMACROCYCLIC LIGAND FOR COPPER-CATALYZED REACTIONS UNDER MILD CONDITIONS

by

Trong Nhan Pham

Submitted in partial fulfillment of the requirements for

Departmental Honors in the Department of Chemistry and Biochemistry

Texas Christian University

Fort Worth, Texas

December 10, 2018

DEVELOPMENT OF A NOVEL POLYAZAMACROCYCLIC LIGAND

FOR COPPER-CATALYZED REACTIONS

UNDER MILD CONDITIONS

Project Approved:

Supervising Professor: Kayla N. Green, Ph.D.

Department of Chemistry and Biochemistry

Onofrio Annunziata, Ph.D.

Department of Chemistry and Biochemistry

Giridhar Akkaraju, Ph.D.

Department of Biology

ABSTRACT. The selective functionalization of C-H bonds under mild and environmental-friendly conditions is a critical step in many major synthetic organic pathways. In 2016, the Serrano-Plana research group introduced a powerful C-H oxidation catalyst, which contains an iron center ligated to a strong-field ***N-methylated*** tetradentate aminopyridine macrocyclic ligand. Also, the Garcia-Bosch research group has shown that copper complexes catalyze the oxidation of alkanes with H_2O_2 in remarkable yields (50-60%). Inspired by their work, this research project focuses on development of a novel catalyst complex that consists of a copper (II) metal center bound to a N-methylated tetra-aza macrocyclic ligand (**Me_3L_2** = 3,6,9-trimethyl-3,6,9,15-tetraazabicyclo[9.3.1]penta-deca-1,11,13-trien-13-ol). It is hypothesized that the N-methylated complex will have stronger electron-donating effect toward the metal center compared to the complex with non-methylated ligand. Moreover, the nitrogen atoms in the methylated complex are protected from the stringent oxidative conditions involving reactive oxygen species. In comparison to the unmethylated L_2 ligand, experimental findings show stronger electron-donating effects from the methyl groups that shift the ^{1}H NMR spectroscopy of the Me_3L_2 ligand upfield. However, the solution of the Me_3L_2 ligand-copper complex, or [Cu(**Me_3L_2**)Cl](ClO_4), in water exhibits identical ultraviolet-visible (UV-Vis) spectroscopic characteristic compared to that of [Cu(**L_2**)Cl](ClO_4). Upon electrochemical analysis in dimethylformamide (DMF) solution with tetrabutylammonium fluoride (TBAF) as an electrolyte, the half-way potential of [Cu(**Me_3L_2**)Cl](ClO_4) was found to be -880 mV (vs. Fc^+/Fc = 0.0 mV). The electrochemical property of [Cu(**Me_3L_2**)Cl](ClO_4) complex suggests both promising catalytic and biological activities that will be further studied.

TABLE OF CONTENTS

ABSTRACT 3

ACKNOWLEDGEMENT 6

LIST OF FIGURES 7

LIST OF SCHEMES 8

LIST OF TABLES 9

INTRODUCTION 10

Introduction to Chemistry and Catalyst 10

Reactions of Coordinated Ligands 11

Bioinorganic chemistry and enzyme mimetics 13

Polyazamacrocycles as ligands 15

Introduction to project 17

EXPERIMENTAL SECTION 22

General Procedures. 22

Instrumentation for Analysis 22

Synthesis of Me_3L_2 (3,6,9-trimethyl-3,6,9,15-tetraazabicyclo[9.3.1]penta-deca-1,11,13-trien-13-ol) 23

Metalation of Me_3L_2 with $Cu(ClO_4)_2$ 24

RESULT AND DISCUSSION 25

Synthesis Scheme for Me_3L_2 and Catalyst 25

Effect of Methylation on ^{1}H NMR Spectroscopy 28

Characterization of zinc(II)-ligand complexes 30

X-Ray Analysis of Metal Complexes 32

UV-Vis Spectroscopic Analysis 36

Cyclic Voltammetry 38

CONCLUSION AND FUTURE DIRECTIONS 40

APPENDIX 41

REFERENCES 52

ACKNOWLEDGEMENT

As an international student, I have always been grateful for being accepted to Texas Christian University and have never doubted my decision to become a member of the Horned Frogs. Firstly, I would like to express my special acknowledgement to Dr. Kayla Green for her guidance as both my research supervisor and mentor within the last three years. In addition to Dr. Green, the faculty members at TCU, including but not limited to Dr. Onofrio Annunziata, Dr. David Minter, Dr. Sergei Dzyuba, Dr. Giridhar Akkaraju, Dr. Claire Sanders, and Dr. Nathanael O'Reilly, have been excellent advisors who helped me envision the type of researcher and teacher I want to become. I also want to thank the members of Dr. Green's research group and graduate students, whose names cannot be all listed here, from the Department of Chemistry and Biochemistry at TCU for creating a healthy research environment where students learn from and work with one another. Last but not least, I would like to thank John V. Roach Honors College and Department of Chemistry and Biochemistry at TCU for giving me an opportunity to present my dedication, hard work and ideas to the public. I will continue to pursue my passion for research and teaching after my graduation, with the ultimate goal of paving the way for the future generation just like what TCU faculties did for me.

LIST OF FIGURES

Figure 1. Template effect of magnesium in DNA synthesis 12

Figure 2. Examples and sub-categories of MPAs 16

Figure 3. Ligand series with unmodified nitrogen atoms 19

Figure 4. Tris-methylated aromatic MPA compounds 20

Figure 5. Proposed mechanism for the Cu-catalyzed oxidation of C–H bonds with H_2O_2 21

Figure 6. Redox cycling of amyloid-copper complex 21

Figure 7. 1H NMR spectra comparison of **Me_3L_2** product 27

Figure 8. ^{1}H NMR spectroscopy comparison between **L_2**, **Me_3L_2**, **L_2·3HCl** and **Me_3L_2·3HCl** . 28

Figure 9. ^{1}H NMR spectrum of Zn(**Me_3L_2**)Cl2 and **Me_3L_2** 31

Figure 10. X-ray crystal structure of [CuCl(**Me_3L_2**)]$^{2+}$ 34

Figure 11. Representation the coordination of Cu^{II} center in a [CuCl(**L**)]$^{2+}$ unit. 35

Figure 12. UV-Vis spectra of CuCl(**Me_3L_2**)ClO_4 solutions in water 36

Figure 13. Cyclic voltammogram obtained for CuCl(**Me_3L_2**)ClO_4 38

LIST OF SCHEMES

Scheme 1. Catalyst provides an alternative pathway. 10

Scheme 2. Mechanism for Eischweiler-Clarke Reaction 18

Scheme 3. One-step synthesis of **Me_3L_2** follows Eischweiler-Clarke methylation. 25

LIST OF TABLES

Table 1. Biological functions of selected metal ions. 15

Table 2. Comparison between ^{1}H NMR resonances of **Me$_3$L$_2$**, **Me$_3$L$_2$·3HCl**, **L$_2$** and **L$_2$·3HCl**. 29

Table 3. Comparison of selected bond angle/^{o} 35

Table 4. Comparison of selected bond length 36

Table 5. UV-Vis spectroscopic properties of CuCl[**L**]ClO$_4$ complexes 37

Table 6. Half-way potential ($E_{1/2}$) values for Cu(II)/Cu(I) redox processes 39

INTRODUCTION

Introduction to Chemistry and Catalyst

Organic chemistry provides access to much-needed molecules for the treatment of disease, development of new materials and devices, and investigation of biochemical pathways. An ongoing challenge in organic chemistry is the discovery of efficient methods, or "green chemistry", to synthesize those target molecules. Green chemistry usually refers to the minimization of unnecessary side products and maximized incorporation of all materials used in the process into the final product.[1]

Catalysts are usually taken into consideration in the design of a "green" synthetic process. A catalyst is typically defined as a compound that accelerates a chemical reaction by providing an alternative pathway.[2] A catalyst is usually recovered after the reaction, also referred as "recyclability" of the catalyst, as illustrated in **Scheme 1**.

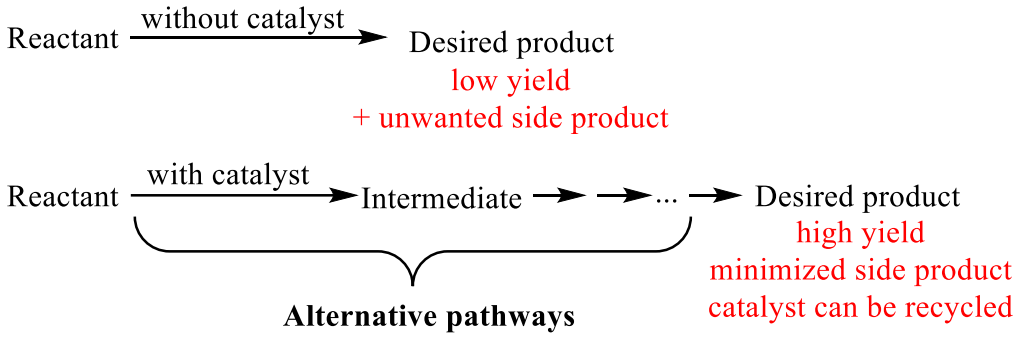

Scheme 1. A catalyst provides an alternative pathway.

Thanks to recyclability, catalysts are usually required in only small amounts, about 0.01 – 20% mol of the starting reagent. Examples of extraordinarily efficient catalysts in nature are enzymes.[3] Metalloenzymes, which are widely represented in almost every group of enzymes,[4] involve the coordination chemistry between organic ligands and inorganic metal centers.

Reactions of Coordinated Ligands

Due to the ability to alter the reactivity of ligands toward external substrates, metal ions are regarded as crucial catalytic centers, even in biology. These metal ion centers are usually strongly bound with organic scaffolds, or ligands, through coordinated bonds to form a complex that might outperform the reactivity of individual components.

One explanation for such reactivity of metal-ligand coordinated complex is the enhancement of the acidity of coordinated ligands. The positively charged metal center can serve as a Lewis acid to stabilize the conjugate basic ligand. In other words, the pK_a values of coordinated ligands are lowered compared to those of free ligands. Thus, substrate molecules in the reaction mixture are more susceptible toward nucleophilic attack. The susceptibility toward nucleophilic attack is no less important biological processes including hydrolysis of esters, amides, carboxylation, and decarboxylation reactions, and transaminations. Equation 1 illustrates the nucleophilic attack on the carbonyl group during hydrolysis of amino-acid esters in human body. Strong nucleophiles like hydroxide ions are rarely found without metal ions at physiological pH. In fact, the uncatalyzed reaction at neutral pH is unobservable.

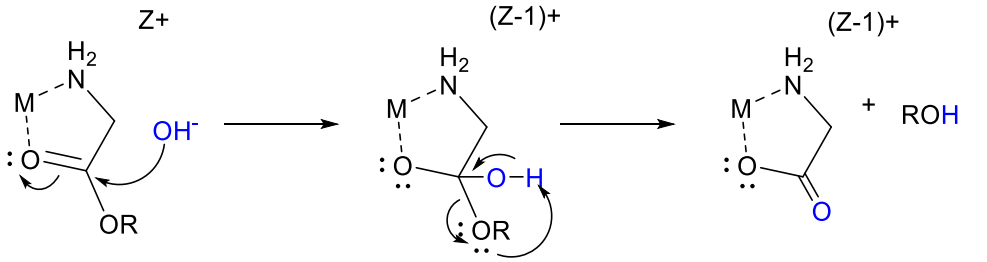

(1)

Another explanation for enhanced performance of coordinated complex as catalyst is the template effect, by which the metal ion center serves to organize reactive units. **Figure 1** demonstrates the role of magnesium in organizing substrates into suitable conformations

required for DNA replication. In this process, the catalytic mechanism involves two Mg^{2+} ions, coordinated to the phosphate groups of the incoming nucleotide triphosphate (NTP) and to three Asp residues. In addition to stabilizing the pentacovalent transition state between DNA polymerase and NTP, Mg^{2+} ions also participate directly in the catalytic process that occurs in the catalytic subdomain of the enzyme. The top Mg^{2+} ion in the figure facilitates attack of the 3'-hydroxyl group of the primer on the α-phosphate of the NTP, while the lower Mg^{2+} ion facilitates the displacement of the pyrophosphate.[5]

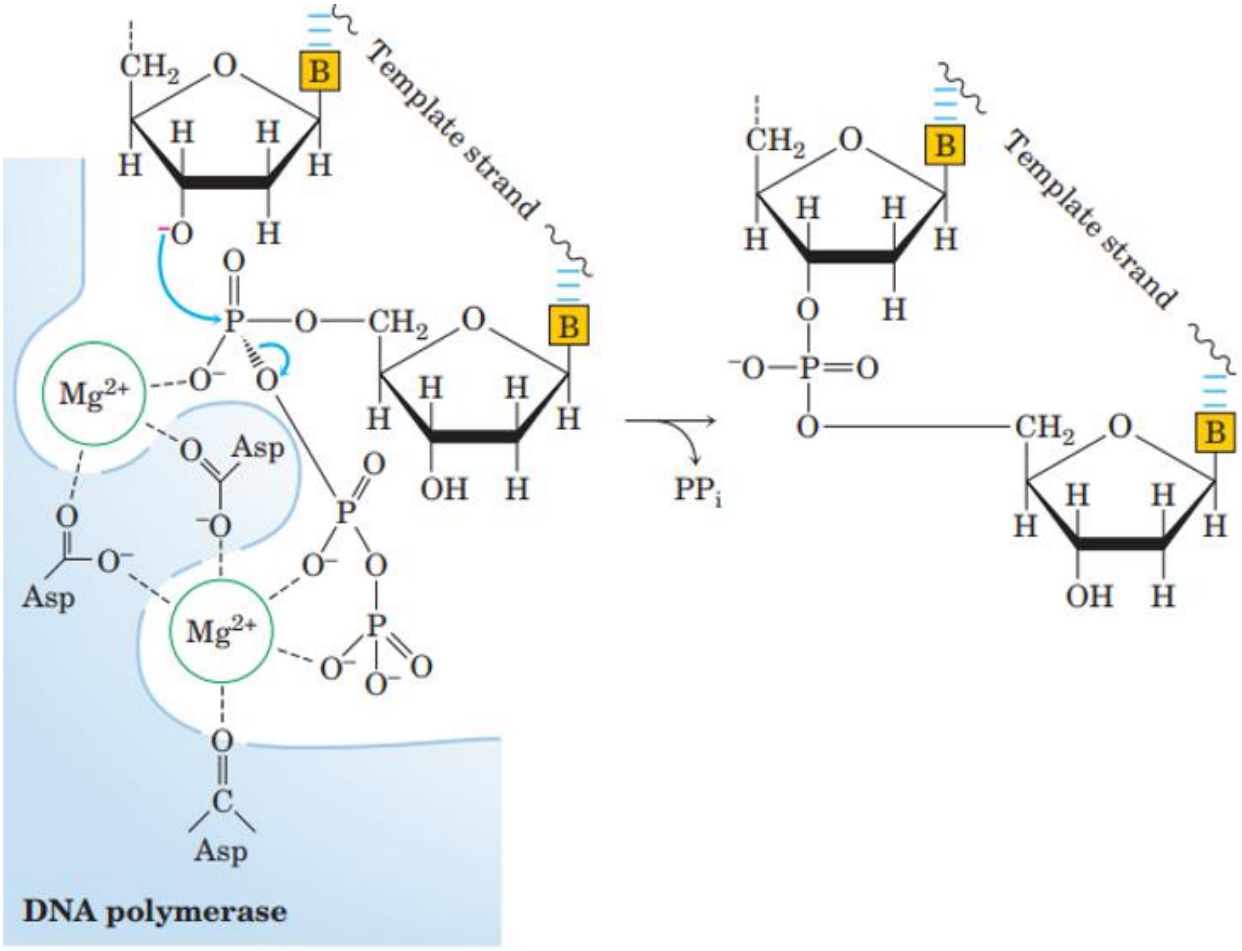

Figure 1. Template effect of magnesium in DNA synthesis.[5]

Bioinorganic chemistry and enzyme mimetics

While metalloenzymes are abundant in nature, the majority of those enzymes in human bodies, usually referred as metallobiopolymers, are enormous and have complex structures. Therefore, obtaining high-resolution structural information and other important physical properties from these metallobiopolymers is typically challenging. Investigating the chemical reactivity of a metal ion center in a metallobiopolymer is also a challenge, since a small change in the structure of coordinated ligand can also affect reactivity. To test a reaction mechanism postulated for the investigated metallobiopolymer, the coordinated ligands need to be modified in a systematic manner, which is difficult even with the biological approach of site-directed mutagenesis.

For these reasons, bioinorganic chemists aim to replicate, as close as possible, the physical and chemical properties of the metal center in a metallobiopolymer by designing model complexes. The field of bioinorganic chemistry depends on two seemingly different, but actually symbiotic disciplines – biology and coordination chemistry. In biology, inorganic elements like metals are as essential to life processes as they are needed in organic chemistry. If the structure of the metallobiopolymer is available through X-ray diffraction analysis, it is possible to design an exact replica of the structure in a model complex, also known as the replicative approach. The development of coordination chemistry in biology cannot be achieved without the discovery of metal centers in biological systems. On the other hand, if the structural information of the metallobiopolymer is unknown, the model approach affords the physical and chemical properties of postulated model complexes to be tested. The model approach in turn provides many valuable insights into structure and mechanism in metallobiochemistry, including the metal-oxidation states, the effects of distance and medium on electron-transfer rates, the roles of steric and

electronic factors, and even the identification of the intermediates in a variety of enzyme-catalyzed reactions.[6] With both approaches, however, it is important to avoid over-interpretation from a model complex during explanation for the physical and chemical properties of the metallbiopolymer. More importantly, the structure of the model complex must be known in detail, which can be accomplished by obtaining high-quality crystal and X-ray diffraction analysis.

Even though the clinical use of organic small-molecules is more widely available, the application of metal complexes as drugs also shows much potential.[7-8] As mentioned above, inorganic elements like metals are not abundant in biological systems, but they can be found in a majority of enzymes in human bodies.[4] Therefore, molecules that have been the result of modeling metalloenzymes have also been used as diagnostic and therapeutic pharmaceuticals. Inorganic elements of central interest to bioinorganic chemists are presented in **Table 1** below. Some metal complexes that are widely utilized in medical applications include, but are not limited to, platinum-based anticancer compounds and technetium diagnostic agents.[9] In short, research in bioinorganic chemistry starts with the postulated design of a ligand, followed by addition of inorganic elements to introduce a model metal-ligand complex for study.

Table 1. Biological functions of selected metal ions.[6]

Metal	Function
Sodium	Charge carrier; osmotic balance
Potassium	Charge carrier; osmotic balance
Magnesium	Structure; hydrolase; isomerase
Calcium	Structure; trigger; charge carrier
Vanadium	Nitrogen fixation; oxidase
Chromium	Unknown, possible involvement in glucose tolerance
Molybdenum	Nitrogen fixation; oxidation; structure
Tungsten	Dehydrogenase
Manganese	Photosynthesis; oxidase; structure
Iron	Oxidase; dioxygen transport and storage; electron transfer; nitrogen fixation
Cobalt	Oxidase; alkyl group transfer
Nickel	Hydrogenase; hydrolase
Copper	Oxidase; dioxygen transport; electron transfer
Zinc	Structure; hydrolase

Polyazamacrocycles as ligands

For medical applications, the metal center needs to be strongly coordinated with the ligand scaffolds to avoid its release *in vivo* that can be caused by the presence of endogenous ligands and metal cations. A class of ligands that form very both thermodynamically and kinetically stable complexes with a variety of metal ion centersare polyazamacrocyclic backbones, or macrocyclic polyamines (MPAs).[10] The prefix "aza" means that selected carbon atoms in a macrocycle (usually nine carbon atoms in the ring at least) are replaced by nitrogen atoms. These nitrogen atoms play crucial rules in the coordination of MPAs with metal ion centers as well. **Figure 2** illustrates examples of MPAs. According to the functional groups in the ring, MPAs can be divided into multiple sub-categories: aliphatic MPAs, aromatic-containing MPAs, macrocyclic polyimines, macrocyclic polyamides, and cryptands.[11]

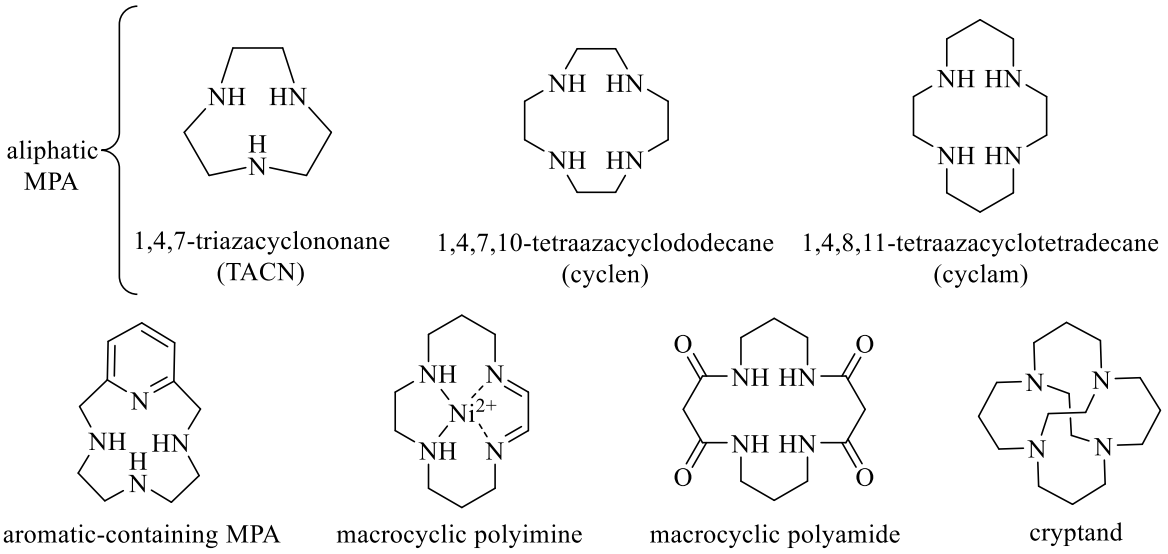

Figure 2. Examples and sub-categories of MPAs.

Functionalization is an important concept behind introducing postulated model ligand scaffolds for the model approach of bioinorganic chemistry. By modifying an existing structure with an unlimited amount of functional groups, new structures with potentially new characteristics of interest are synthesized and studied. The introduction of a pyridine motif to form an aromatic-containing MPA has led to a novel ligand scaffold group, with distinctive physical properties and catalytic capabilities of great interest in recent years.[12] The field of application of aromatic-containing MPAs ranges from biology to supramolecular chemistry, encompassing MRI, molecular recognition, materials and catalysis. Hypothetically, the increased conformational rigidity from the aromaticity of pyridine ring allows the characterization of metal complexes in high oxidation states, along with the study of catalytic behavior in oxidation reactions.

The rigidity of MPA-metal complexes can be further specialized for particular applications by modification of nitrogen atoms in the macrocyclic ring. For example, DOTA (also known as tetraxetan), which consists of a central twelve-membered tetra-azamacrocycle

with pendant carboxylic arms on nitrogen atoms is used as gadolinium-based MRI contrast agent.[13] Recent publication by Le Fur *et al.*[14] also presented yttrium(III) complexes with pyclen-based ligands (a subtype of aromatic MPAs) bearing pendant picolinate arms that might surpass the current ^{90}Yttrium-DOTA complex as potential radiopharmaceuticals. While the introduction of functional groups can increase chelating effect of a ligand by providing more rigidity, the bulky conformation of the three-dimensional structure of ligand scaffold might prevent nitrogen atoms from approaching metal ions. Because of the various coordination numbers associated with different oxidation states, some metal ions can find their most suitable accommodation in space to form a stable complex with the corresponding ligands despite steric effects, while some metal ions require a more strict coordination environment for complexation. The trend for relative stabilities of complexes formed by metals are generalized through the Irving-Williams series: $Cu^{2+} > Ni^{2+} > Co^{2+} > Fe^{2+} > Mn^{2+}$. Indeed, the ligand introduced in this work can form high-quality crystals, suitable for further characterization, with copper (II) perchlorate in mild condition, while crystals for iron (III) complexes were not obtained and the behaviors of ligand-iron (III) could not be further studied.

Introduction to project

This project follows the model approach of bioinorganic chemistry to introduce a new ligand through functionalization of existing ligand library published by the Green's research group.[15-16] As mentioned previously, functionalization of N atoms has been a central part for development of new ligand in recent years. Motivated by the work of Serrano-Plana[17] and Bongki Shin,[18] the Eischweiler-Clarke methylation of nitrogen atoms is the foundation of ligand synthesis in this project. The generalized mechanism of Eischweiler-Clarke methylation is illustration in **Scheme 2**.

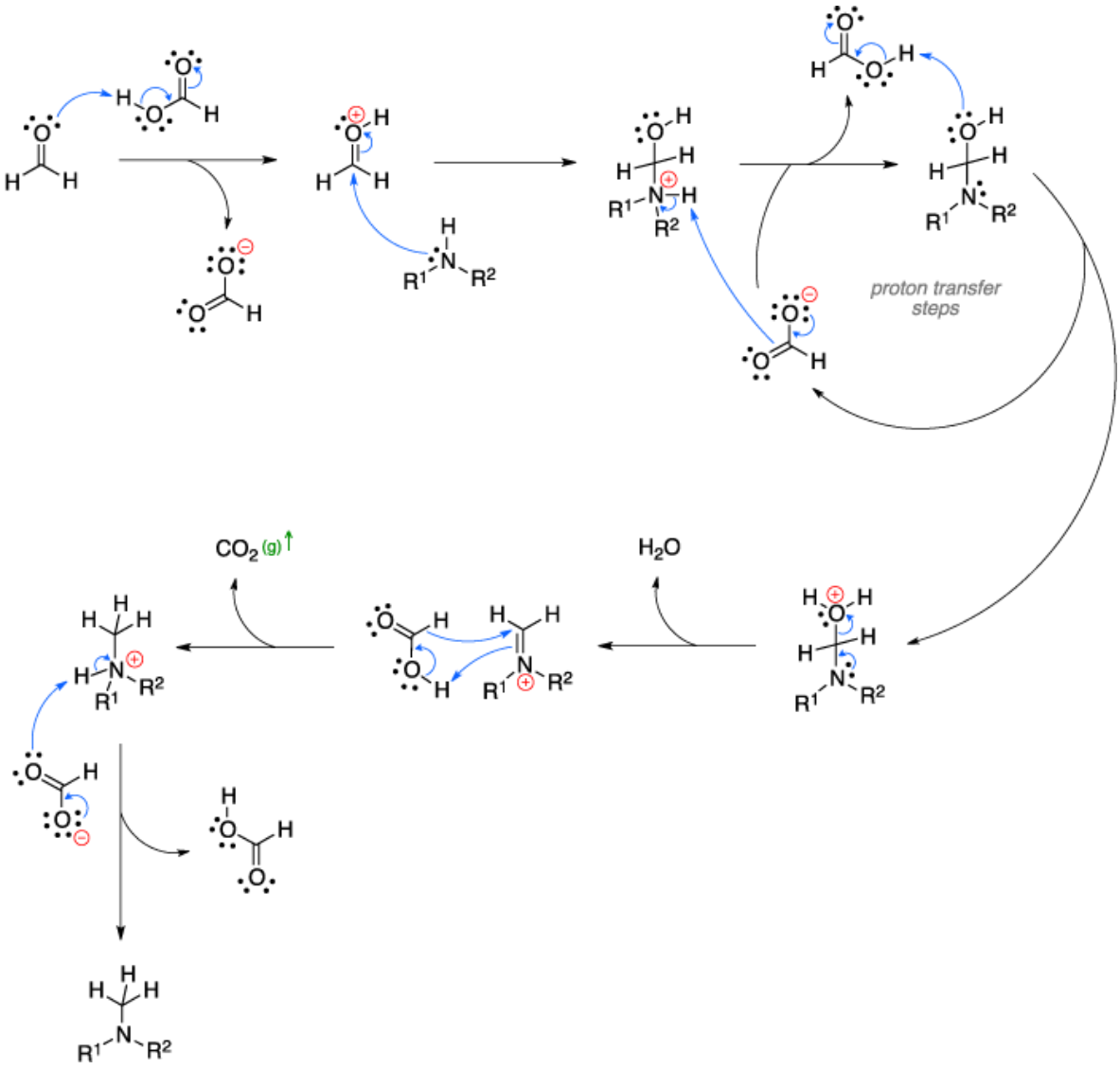

Scheme 2. Mechanism for Eischweiler-Clarke Reaction.[19]

The driving force of Eischweiler-Clarke methylation is the formation of an imine intermediate, which can only be accomplished by nitrogen atoms. There are three benefits associated with the Eischweiler-Clarke methylation that conform to the twelve principles of green chemistry.[1] First, besides the unmethylated amine, the only other reagents required are formaldehyde and formic acid, both of which are commercially available and easily removed after the reaction is complete. Since the goal is to fully methylate all primary and secondary amine groups in the pyclen series, an excessive amount of starting reagent can be used to avoid

incomplete side product. Second, the methylation is site-directed, and occur(s) only at primary and secondary amine. Therefore, if nitrogen-atom modification is the only purpose of molecule functionalization, other atoms in the molecule with sufficient electron density that can act as a nucleophile, like oxygen, are inert toward the reaction. Last but not least, the only side product of this reaction is carbon dioxide. This is also thanks to the imine intermediate which reacts with formic acid to form the final amine product with the release of gaseous carbon dioxide as driving force. Unlike combustion, only one molecule of carbon dioxide was released for one molecule of reacted amine, carbon monoxide cannot be formed and no oxygen was involved in the reaction, so this is not a significant environmental issue.

The target of methylation in this research is **L_2** (chemical structure illustrated in **Figure 3**), which is the pyclen with hydroxyl functional group at –para position on the pyridine ring. Because water solubility has always been one of the major goals of developing compounds for medical applications, **L_2** is the perfect fit for Eischweiler-Clarke methylation, which does not affect the hydroxyl functional group. Previous published work has only been focusing on methylation of pyclen and *p*-methoxy pyclen (as illustrated in **Figure 4**).[17] Synthesis of **L_2** was followed by previous publications;[16] thus, this will not be further discussed. Ligand series with unmodified nitrogen atoms published by the Green research group is illustrated in **Figure 3**.

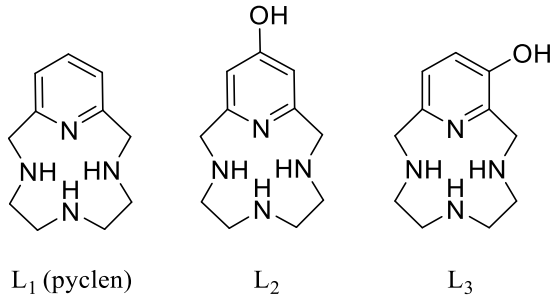

Figure 3. Ligand series with unmodified nitrogen atoms published by the Green research group.

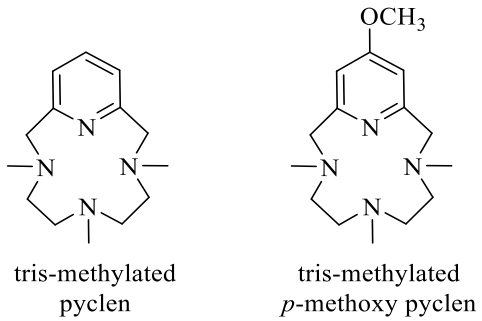

Figure 4. Tris-methylated aromatic MPA compounds that have been recently published.[17]

The next step in the model approach to introduce a novel metal-ligand complex is to choose a suitable metal ion for complexation and study. Iron (III) metal center was originally chosen for study to elaborate the work of Serrano-Plana,[17] but the difference in solubility of ligands and the challenge with coordination of iron center, turn the research interest toward complexation with different metal centers. Copper (II), with the greatest coordination capability among transition metals, according to the Irving-Williams series, but no less important applications in catalysis and medicine, as suggested in **Table 1**, becomes the central focus of introducing a new catalytic complex in this work. Indeed, copper-centered catalysts with MPAs has also been recently focused to mimic the ability to regulate Fenton-type redox reactions of enzymes.[20] Hereby, a novel copper-centered complex, CuCl(**Me$_3$L$_2$**)ClO$_4$ with a novel ligand model (Me$_3$L$_2$) as chelator is synthesized and studied for new physical properties in comparison to those of published complexes. The physical properties analyzed with nuclear magnetic resonance (NMR) spectroscopy, ultraviolet-visible (UV-Vis) spectroscopy, cyclic voltammetry, and X-ray diffraction, showed that while there is no significant change in the three-dimensional structure of the complex, the notable difference in the Cu^{II}/Cu^{I} redox coupling of the complex might suggest different catalytic and biological behaviors of the CuCl(**Me$_3$L$_2$**)ClO$_4$ as a new model catalyst. In particular, Cu^{I} oxidation to Cu^{II} has been proposed by Garcia-Bosch *et al.*[20] as part of the mechanism (as illustrated in **Figure 5**) for the catalytic activity of copper-catalysts

toward C-H peroxidation with H_2O_2, resulting in an important intermediate prior to alcohol formation. On the other hand, Cu^{II} reduction to Cu^{I} of copper-amyloid complex could inhibit the production of reactive oxygen species, which is a part of neurodegenerative disorders' pathology involving coordination between amyloid β and metal ions. The Cu-ascorbate redox system (in presence of high levels of oxygen and ascorbate, as illustrated in **Figure 6**), which was described by Faller and co-workers,[21] has been employed by many research groups[22-25] to determine if the model ligands could act as inhibitors by forming stable Cu^{I} complex that is harder to undergo oxidation.

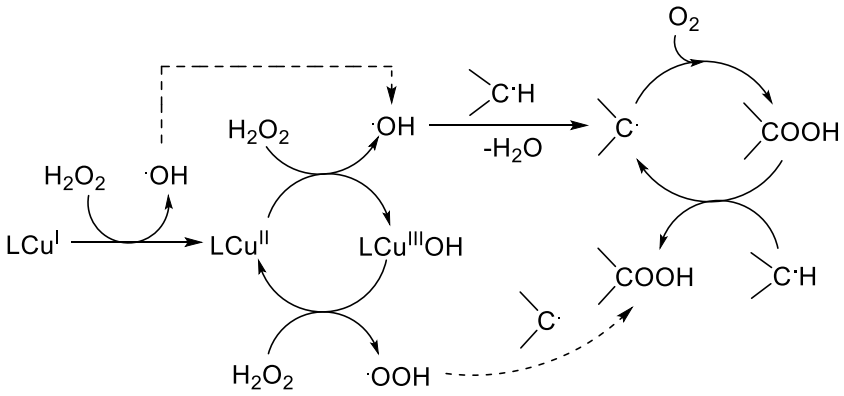

Figure 5. Proposed mechanism for the Cu-catalyzed oxidation of C–H bonds with H_2O_2 (Fenton-type regime).[20]

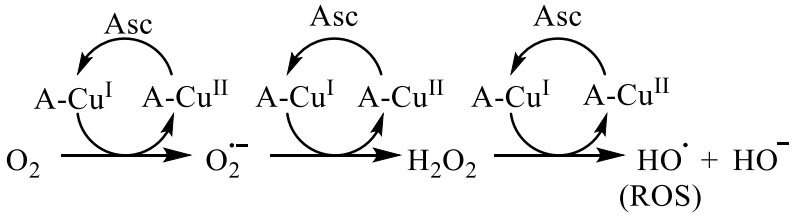

Figure 6. Redox cycling of amyloid-copper complex (A-Cu) in the presence of oxygen and ascorbate to produce reactive oxygen species (ROS).[21]

EXPERIMENTAL SECTION

General Procedures.

All reagents were purchased from commercial sources and used as received, unless noted otherwise. **L_2·3HCl** salts were synthesized following methods reported by the Green Research Group.[15-16]

Instrumentation for Analysis

All nuclear magnetic resonance (NMR) experiments were run with a Bruker Advance III HD 400 MHz spectrophotometer. ^{1}H NMR chemical shifts were adjusted using the deuterated solvent peak as reference. The referent value for D_2O is 4.79 ppm, as reported in Fulmer, 2010.[26]

All ultraviolet-visible (UV-Vis) spectroscopic experiments were recorded on a 8453 Agilent spectrophotometer within the range 200-800 nm. A 1-mL quartz cuvette with the path length of 1 cm was used to contain the solution for measurement.

A Leica MZ 75 microscope was used to observe and isolate crystals suitable for X-ray diffraction analysis. The single crystal of CuCl[**Me_3L_2**]ClO_4 was mounted on the goniometer of the diffractometer using Paratone-N oil (cryoprotectant) on the tip of MiTeGen MicroLoops LD™.

A Bruker D8 Quest diffractometer was employed for crystal screening, unit cell determination, and data collection; which was obtained at 100 K under the flow of liquid nitrogen using Oxford Cryosystem. The goniometer was controlled using the APEX-2 software suite, v.2014.11-0.[27] The samples were optically centered with the aid of video camera so that no translations were observed as the crystal was rotated through all positions. X-ray radiation was generated from a Molybdenum K_α sealed X-ray tube (λ = 0.71076 Å) with a potential of 50 kV and a current of 30 mA; filtered through a graphite monochromator in the parallel mode (175

mm collimator with 0.5 mm pinholes). The intensities of diffracted X-rays were collected with a Photon 100 CMOS detector. The crystal-to-detector distance was set to 50 mm.

The X-ray diffraction experiment setup was programmed with the assistance of the APEX-3 software.[28] For CuCl(**Me_3L_2**) ClO_4 crystal, X-ray diffraction experiment was performed with an exposure time of 10 seconds and a scan angel of 5° per frame. While preliminary screening and computational algorithms assigned the crystal with monoclinic space group, the X-ray diffraction experiment was executed following the program on APEX-3 for triclinic space group with lower symmetry in order to obtain a data package with 100% completeness for further refinement. The collected diffraction frames were integrated as a monoclinic space group with the Bruker SAINT Software package[29] using a narrow frame algorithm. Data were then corrected for absorption effects using the multi-scan method SADABS.[30] Finally, the crystal structure was solved with the ShelXS[31] structure solution program using direct methods and refined with the ShelXL[32] refinement program using least-squares minimization. Hydrogen and non-hydrogen atoms were refined using anisotropic thermal parameters. All structure solution and refinement works were performed using Olex2.[33]

Synthesis of Me_3L_2 (3,6,9-trimethyl-3,6,9,15-tetraazabicyclo[9.3.1]penta-deca-1,11,13-trien-13-ol). A mixture of formaldehyde 37% (2.32mL, 30.97 mmol) and formic acid 88% (1.35mL, 30.98 mmol) was added dropwise to **L_2·3HCl** (670 mg, 1.99 mmol) at 0°C. The reaction mixture was stirred for 1 hour at room temperature, resulting in a brown solution. The solution was then heated to 105°C for an additional 2 hours. The solution was allowed to cool to room temperature and the pH was adjusted to 14 with a NaOH 30% solution. Solvent was removed under reduced pressure. The resulting light yellow solid was dissolved in cold isopropanol, then filtered through

a 0.2 μm Nylon filter. The filtrate was then reduced under vacuum to obtain the product as a yellow solid. Yield = 74.5% (398 mg, 1.51 mmol). ^{1}H NMR (400 MHz, D_2O) δ 6.36 (s, 2H), 3.61 (s, 4H), 2.64 (t, 4H), 2.48 (t, 4H), 2.38 (s, 6H), 2.30 (s, 3H). MS (75mV, in H_2O) (m/z) Found: 265.0826 $[Me_3L_2+H^+]^+$ (100%). Theoretical: 265.2028 $[Me_3L_2+H^+]^+$.

Metalation of Me_3L_2 with $Cu(ClO_4)_2$. Me_3L_2 (49.8 mg, 0.188 mmol) was dissolved in 10 mL H_2O resulting in a basic solution with pH 11.8, which was then adjusted to 7.92 with a HCl 1M solution. Next, $Cu(ClO_4)_2 \cdot 6H_2O$ (69.8 mg, 0.188 mmol) was dissolved in 2 mL H_2O and was then added slowly to the stirring solution above to yield a blue solution with pH equal to 2.51. The reaction mixture was stirred overnight in a loosely capped 20-mL vial. Upon completion, the solution was centrifuged and the supernatant was dried by removing solvent under reduced pressure. The resulting blue solid was then dissolved in acetonitrile, followed by centrifugation and filtration through a 0.2 μm nylon filter twice to isolate the insoluble contaminant salts. The filtrate was dried by removing solvent under pressure to obtain a green crude product. The crude product was dissolved in 2 mL H_2O and blue high-quality crystals were obtained after three days by utilizing slow evaporation of water. These crystals will be used for X-ray diffraction analysis, UV-Vis spectroscopy and electrochemical characterizations.

RESULT AND DISCUSSION

Synthesis Scheme for Me_3L_2 and Catalyst

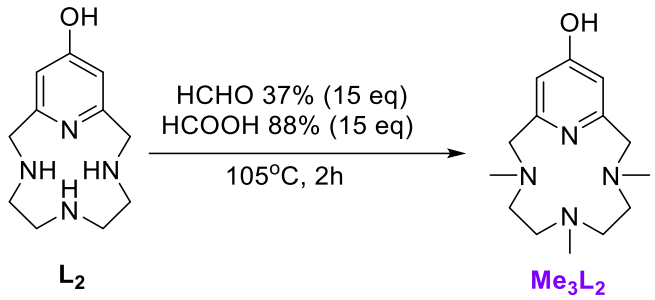

Scheme 3. One-step synthesis of Me_3L_2 follows Eischweiler-Clarke methylation.

L_2·3HCl salt has been synthesized following the procedure published by the Green's research group[15-16] and can be immediately used as starting reagent for methylation, as illustrated in **Scheme 3**. One advantage of the Eischweiler-Clarke reaction is that the methylation is site-directed and only occurs at the nitrogen atoms thanks to the formation of an imine intermediate. Therefore, side products involving oxygen centers from the hydroxyl functional group are not part of the product. Despite this, methylation of the pyclen series has only been performed on a limited number of compounds, including pyclen and *p*-methoxy pyclen (**Figure 4**). The result in this work shows that there is no need to protect the oxygen atom from the hydroxyl group prior to methylation. Thus, the important feature of promoting water solubility from the hydroxyl group is still retained in Me_3L_2 while avoiding a three-step approach (protection, methylation and deprotection) toward the final product. Even though the synthesis of L_2 involves a protection and a deprotection step with the benzoxy group, these steps are necessary for the cyclization between the pyridinophane ring and amine to form a 12-membered ring pyclen.

An excess amount (15 equivalents) of formaldehyde 37% and formic acid 88% is necessary to ensure complete methylation of all three secondary amines in **L_2**, but both of these

reagents are commercially available and more essentially, only carbon dioxide was produced as side product. Published procedure from Serrano-Plana group noted the use of 300 equivalents of formaldehyde 37% and 80 equivalents of formic acid 88%, followed by heating at 105℃ for two hours, during preparation of methylated pyclen (Me_3L_1), but this excessive amount of reagents and heating time seems unnecessary. As suggested by Bongki Shin *et al.*[18] in their attempts to synthesize **Me_3L_1** in 2015, heating at 105℃ for two hours is necessary to reflux the reaction mixture produce fully methylated product, which was verified by mass spectroscopic analysis at one-hour intervals.

In the purification step, the excess formaldehyde (boiling point is -19˚C at 1 atm) can be removed under reduced pressure along with water (boiling point is 100˚C at 1 atm). Formic acid can be neutralized with a solution of NaOH 30%, but the formation of formate salts (HCOONa) should also be removed. The formate salt byproduct was observed in the NMR spectra of the crude product as a resonance near 8.465 ppm. Due to the presence of the hydroxyl group on the pyridine ring, **Me_3L_2** is hypothetically more hydrophilic than the **Me_3L_1** or **Me_3L_{MeO}** reported previously by Serrano-Plana's group. In fact, **Me_3L_2** was found to be less soluble in organic solvents like dichloromethane (DCM) compared to **Me_3L_1**. Therefore, it is more challenging to purify **Me_3L_2** using silica-based chromatography with DCM as part of the mobile phase. However, a different purification method is feasible. Since HCOONa is the only possible impurity, repeated wash of the crude product with cold isopropanol, in which **Me_3L_2** was more soluble compared to formate salts, followed by filtration and solvent removal under reduced pressure, is sufficient to obtain a clean product (as illustrated in **Figure 7**).

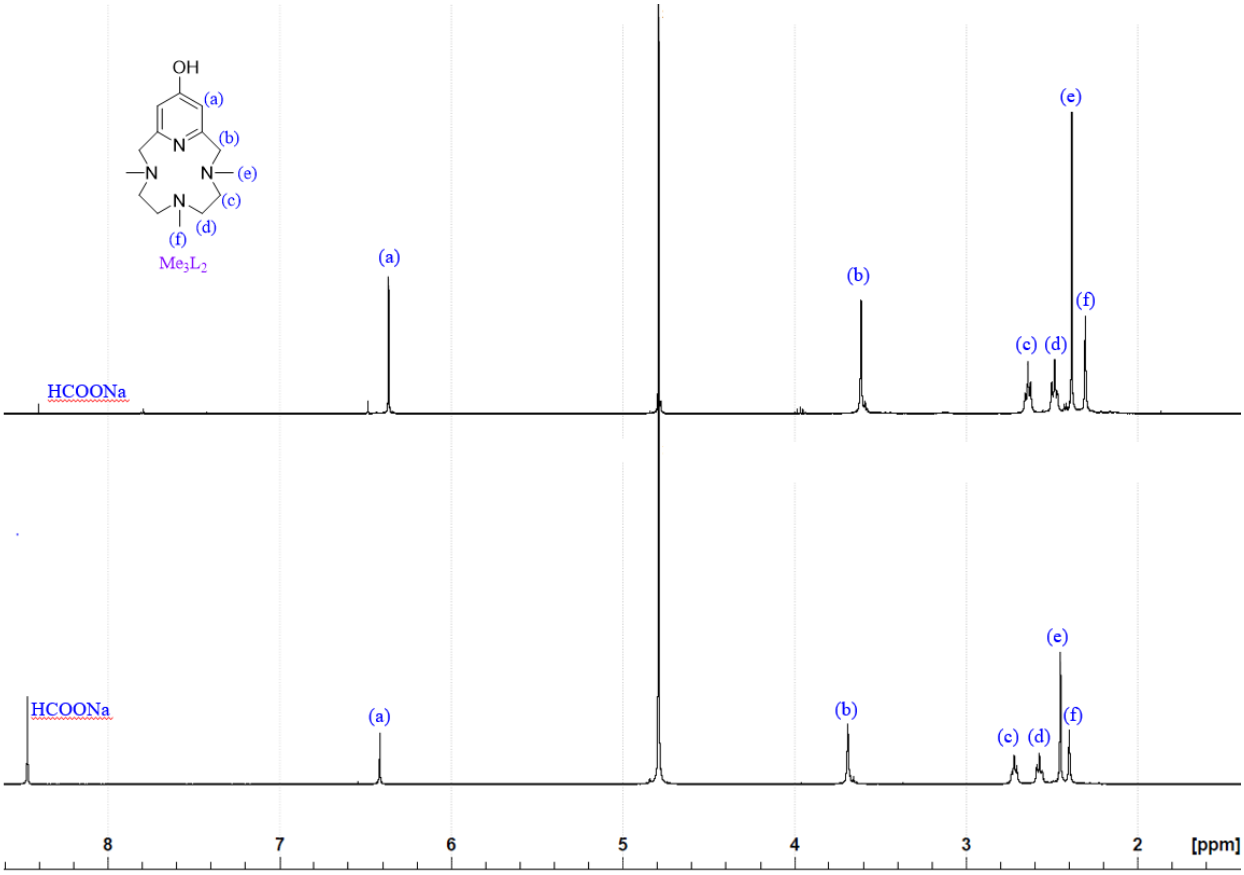

Figure 7. 1H NMR spectra comparison of Me_3L_2 product in D2O before purification (top spectrum) and after purification (bottom spectrum).

Initially, repeated attempts were performed to chelate **Me₃L₂** scaffold toward iron (II) and iron (III) centers. However, X-ray quality crystal of **Me₃L₂**·Fe complex were not obtained despite promising results from MS spectra. The coordination between **Me₃L₂** and iron might require a more carefully controlled environment for complexation, as suggested by the Irving-Williams series in the introduction. On the other hand, copper (II) perchlorate was sufficient to form a complex overnight with **Me₃L₂** in water. Only pH needs to be carefully controlled (modified to 7.92) during the reaction because **Me₃L₂** is basic in water (pH = 11.8) and copper (II) hydroxide might be formed instead of the desired complex. Since cupric ion (Cu^{2+}) is a Lewis acid, pH of the resulting reaction mixture drops to 2.51 after stirring overnight. The solid

state structure of the copper-**Me$_3$L$_2$** complex, CuCl(**Me$_3$L$_2$**)ClO$_4$ was obtained as stated in the above-mentioned procedure.

Effect of Methylation on ^{1}H NMR Spectroscopy

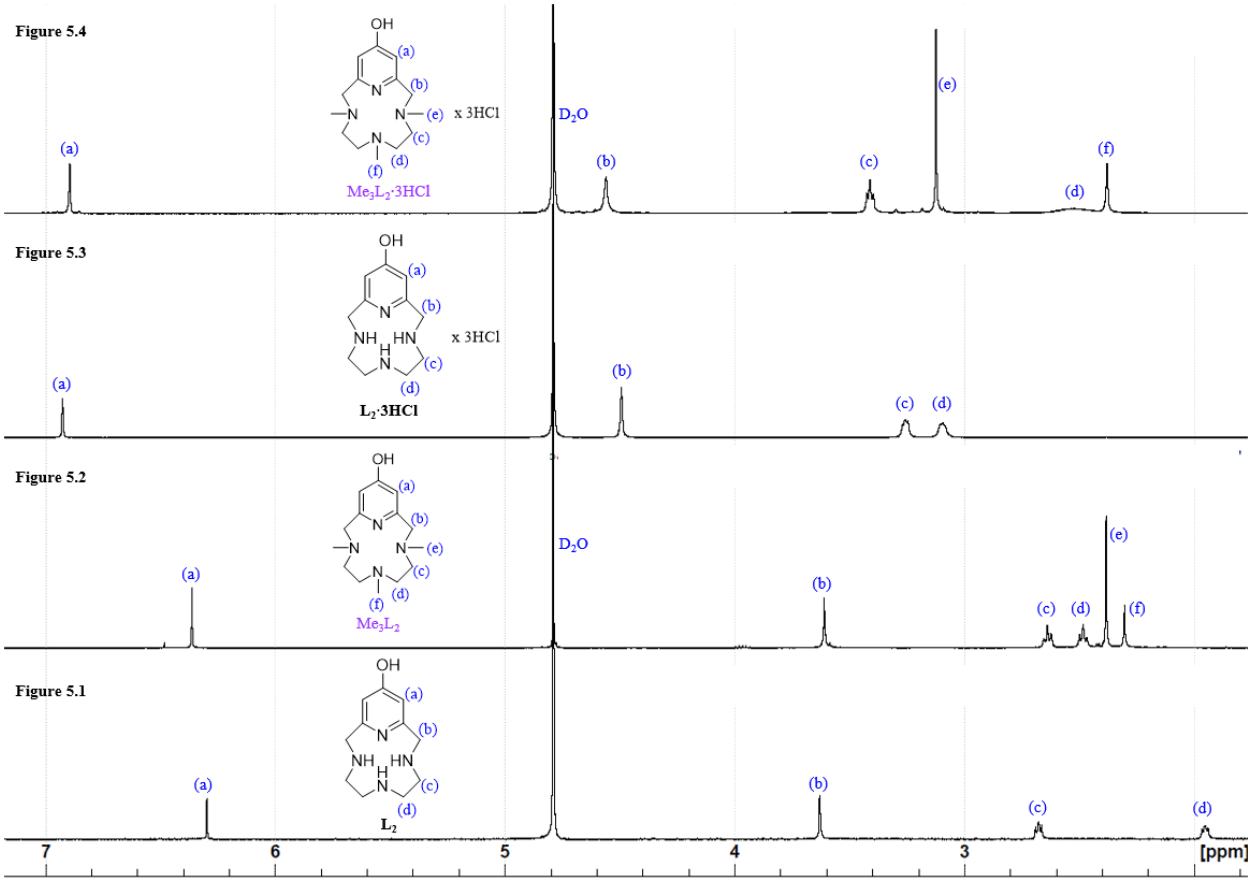

Figure 8. ^{1}H NMR spectroscopy comparison between **L$_2$** (Figure 8.1), **Me$_3$L$_2$** (Figure 8.2), **L$_2$·3HCl** (Figure 8.3) and **Me$_3$L$_2$·3HCl** (Figure 8.4). All samples were obtained in deuterated water (D_2O) solvent. pH of L_2 and Me_3L_2 samples are 14 and 11.8, respectively. NMR spectra are calibrated with D_2O singlet peak at 4.79 ppm.

Identification and purity of the newly synthesized ligand, **Me$_3$L$_2$**, was assessed using ^{1}H NMR spectroscopy. Numerical values of the frequency where signaling peaks of both compounds occurred were recorded in the table below. Because ^{1}H NMR of the L_2 was taken in

the acidified form, **L_2·3HCl**, the ^{1}H NMR spectrum of **Me_3L_2** after acidification to pH of 2, followed by solvent removal and dissolution in D_2O, was also included. The effects of the introduced methyl groups on NMR chemical shifts will be further investigated.

Table 2. Comparison between ^{1}H NMR resonances of Me_3L_2, Me_3L_2·3HCl and L_2·3HCl

Proton label	Me_3L_2	Me_3L_2·3HCl	L_2	L_2·3HCl
(a)	6.36	6.90	6.30	6.93
(b)	3.61	4.56	3.63	4.39
(c)	2.64	3.41	2.68	3.26
(d)	2.48	2.53	1.95	3.10

While NMR spectroscopy can be a powerful tool for the study of electronic effects of functional groups on atomic nuclei through chemical shifts of detected resonances, the environment of an NMR sample might interfere with the chemical shifts of interest. Comparison between ^{1}H NMR spectra of **Me_3L_2** in deprotonated and fully protonated (**Figure 8** and **Table 2**) form shows large differenced in both chemical shifts and clarity of the multiplicity of each resonance. In terms of chemical shifts, all six proton resonances (a)-(e) from **Me_3L_2** all shift further downfield upon protonation. This observation is expected since protonation de-shield the electron density across the molecule, as well as proton nuclei. In addition, acidic environment can also increase the proton-exchange rate of protons of the analyzed compound, which gives rise to a broad signal instead of a resolved multiplet signal. As a result, proton resonance corresponding to position (d) appears as a broad signal in both spectra of **Me_3L_2·3HCl** and **L_2·3HCl**, instead of a triplet as observed in the spectrum of **Me_3L_2** and **L_2**. According to Figure 8.4, not only the broad resonance of (d) overlaps with (f), which makes resonance integration less accurate, the assignment of these two signals to whether position (d) or (f) on the structure is also ambiguous. As protons at position (d) can couple with two protons at position (c) to give triplet signal, the ^{1}H NMR spectra of deprotonated form of **Me_3L_2** (Figure 8.2) and **L_2** (Figure

8.1) is more useful for proton assignments. Proton signal comparisons between ^{1}H NMR spectra of **Me$_3$L$_2$** and **L$_2$** as listed in **Table 2** showed only one significant variation associated with protons at position (d), with $H_d^{Me_3L_2}$ signal occurs more downfield with respect to $H_d^{L_2}$, which is not consistent with the shielding effect of the methyl groups on nitrogen atoms, given how large the difference is (0.53 ppm). This irregularity might be due to the difference in pH of both samples (14 for **L$_2$** and 11.8 for **Me$_3$L$_2$**), along with the presence of sodium chloride salts and hydroxide ions presence in **L$_2$** sample after basification of **L$_2$·3HCl**, which affect the magnetic field surrounding proton (d). Thus, in this case, ^{1}H NMR spectroscopy is only used as a detection method to verify the purity of the product, not as an indication of the electronic effect of the methyl groups on the free ligand **L$_2$**, though ^{1}H NMR spectroscopy of more pH-controlled samples is feasible.

Characterization of zinc(II)-ligand complexes

Before moving on to X-ray diffraction analysis of CuCl(**Me$_3$L$_2$**)ClO$_4$ complex, it is important to note that there are more than one way to identify the three-dimensional structure of a ligand-metal complex of interest. While X-ray diffraction provides the most accurate three-dimensional structural information, achieving X-ray quality crystals sometimes proves to be challenging. Not only the crystallization set-up needs to be almost free of any impurities, but also a structure that can diffract X-ray to give detectable diffracting patterns for analysis is necessary.

While the majority of metal ions of interest are paramagnetic with slow electron-spin relaxation times that might broaden resonances beyond recognition, NMR spectroscopic methods have been highly useful in bioinorganic chemistry as much as other chemistry disciplines. From ^{1}H and, to a lesser extent, ^{13}C, ^{15}N, and ^{31}P NMR spectra, information about the three-dimensional structure of biopolymers, including metal-bound ions, can be obtained.[6] While

NMR analysis of complexes containing paramagnetic metal ion is feasible, presented here is the ^{1}H NMR analysis of a more simple metal complex with zinc (II), a diamagnetic metal ion, which does not affect the conventional range of resonances (from 0 to 12 ppm).

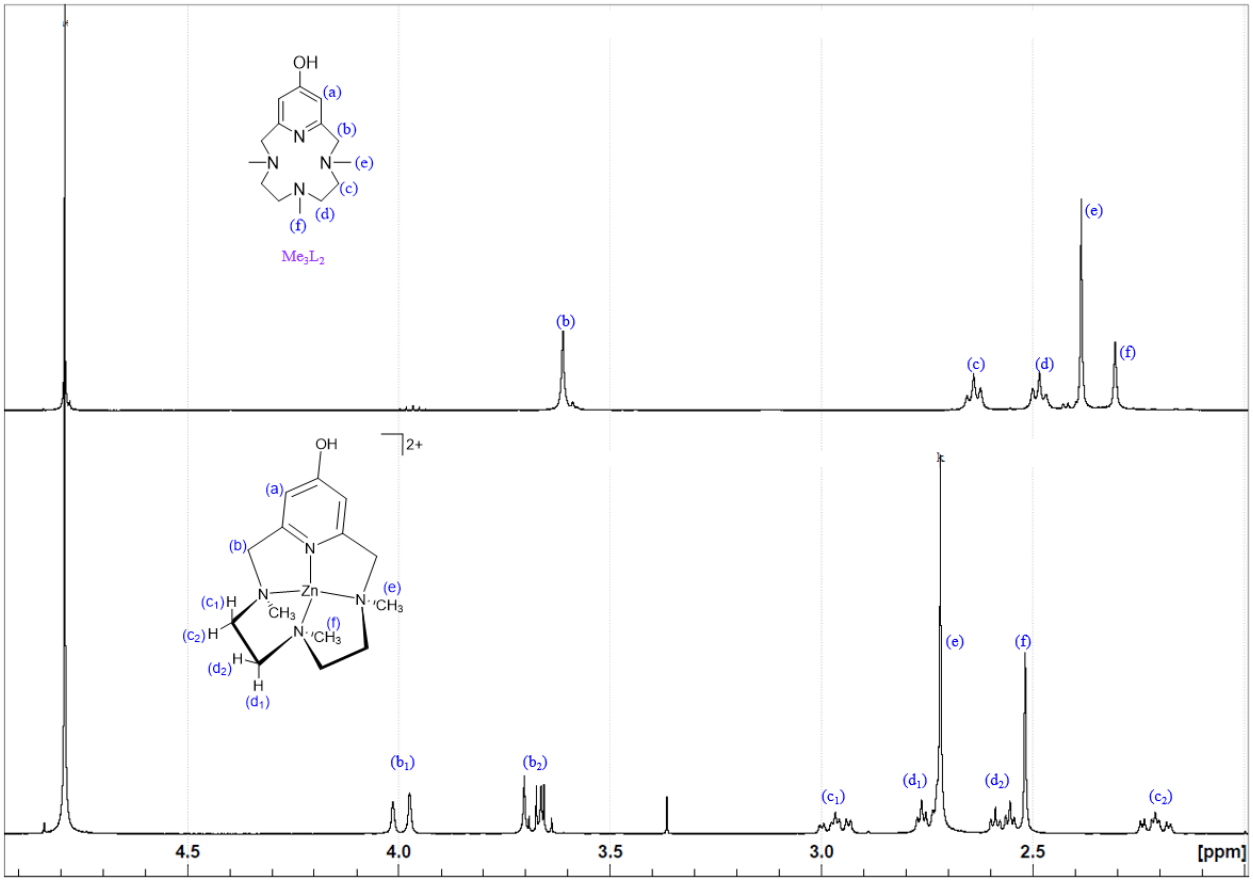

Figure 9. ^{1}H NMR spectrum of Zn(**Me$_3$L$_2$**)Cl2 (bottom) and **Me$_3$L$_2$** (top).

Resonance splitting and multiplicity can be used as implication of the rigidity of the complex, which is less symmetric than the free ligand. Resonance splitting occurs when one signal associated with more than two protons is split into more than two distinguishable signals upon environmental change in the NMR sample. Multiplicity is the coupling of neighboring distinguishable protons to give a multiplet instead of singlet; for example, protons at position (c) and (d) coupling to one another to give two triplets in the top spectrum of **Figure 9**. Both phenomena, resonance splitting and multiplicity, are direct results of the appearance of

distinguishable protons. As the structure of **Me_3L_2** becomes more rigid, rotation of C-H bonds originating from one carbon atom, even a sp^3 carbon atom, becomes more inhibited. The two protons at each position (b), (c), and (d) in **Me_3L_2** now have fixed positions, and thus become distinguishable in the complex with zinc chloride. Since zinc chloride was only added to the NMR sample to evaluate the coordination ability of Me_3L_2 with ^1H NMR spectroscopy and the central focus is copper-centered complex, further characterization of the zinc (II) complex was not yet performed, which can give accurate J-J coupling constants calculation and proton assignments. With this result, it was expected that copper (II) centered complex retains the coordination rigidity.

X-Ray Analysis of Metal Complexes

X-rays have wavelengths of 1 Å, close to that of interatomic distances. Therefore, X-ray crystallography offers the most powerful structure probe of macromolecular structure, including metal coordination geometries. However, structural determination using X-ray diffraction depends on the availability of a translationally ordered sample – a single crystal, to diffract X-ray. Because of this reason, protein crystals, which have high water content and usually highly disordered compared to small molecule crystals, do not diffract X-rays as well.

Structure solution and refinement of crystalline CuCl(**Me_3L_2**)ClO_4 showed that the unit cell of the CuCl(**Me_3L_2**)ClO_4 complex was composed of two $[CuCl(\mathbf{Me_3L_2})]^{2+}$ complexes, two perchlorate counter-ions and one H_2O molecule. Chloride ions come from the HCl 1M solution used to adjust pH of Me_3L_2 in water from 11.8 to 7.92 prior to metalation. Because this study focus on the metal-ligand coordination, only the crystallographic structure of the $[CuCl(\mathbf{Me_3L_2})]^{2+}$ is described and illustrated below (**Figure 10-11** and **Table 4-5**). Though this result also shows that N-methylated ligand can easily form complex with copper (II) center in mild condition (reaction was run overnight at room temperature and pH below 8), the main

concern is whether newly introduced methyl groups have any effect on the three-dimensional structure of the complex.

While the coordination geometry of the copper (II) center is the same between $[CuCl(\mathbf{Me_3L_2})]^{2+}$ and $[CuCl(\mathbf{L_2})]^{2+}$, a five-coordinate copper-centered geometry, not all bond lengths and angles remain the same. Bond length data in Table 5 shows that the distances between copper (II) center and three methylated nitrogen atoms increase in $[CuCl(\mathbf{Me_3L_2})]^{2+}$ in comparison to the distances between similar atoms in $[CuCl(\mathbf{L_2})]^{2+}$. The increase in distance from copper (II) center to N_2, N_3 and N_4 are 0.03, 0.09, and 0.03 Å, respectively. On the other hand, the distance between copper (II) center to N_1 and Cl_1 remains almost unchanged (less than 0.01 Å) between the two complexes. This means that the distance from copper (II) center to coordinating atoms have increased in $[CuCl(\mathbf{Me_3L_2})]^{2+}$ complex. This result is within expectation according to the steric effect of the introduced methyl groups on nitrogen atoms.

Further investigation of bond angles shows that while the copper (II) center favors a location away from the methylated nitrogen atoms, especially N_3, this provides more available space on the chloride-coordinating site, with N_1-Cu_1-N_3 angle is lower in $[CuCl(\mathbf{Me_3L_2})]^{2+}$ (96.117°) in comparison to that of $[CuCl(\mathbf{L_2})]^{2+}$ (98.896°). Thanks to more available space, chloride atom coordinating to the copper (II) center does not need to locate further from the methylated N_3 atom to avoid steric effect. Indeed, the N_3-Cu_1-Cl_1 angle is much smaller in $[CuCl(\mathbf{Me_3L_2})]^{2+}$ (97.605°) in comparison to that of $[CuCl(\mathbf{L_2})]^{2+}$ (106.915°). Consequently, the the N_1-Cu_1-Cl_1 angle is much larger in $[CuCl(\mathbf{Me_3L_2})]^{2+}$ (166.205°) in comparison to that of $[CuCl(\mathbf{L_2})]^{2+}$ (154.205°). This structure might allow copper (II) centers to coordinate with a sixth atom, an important structural feature of a catalytic complex that is to have multiple coordination

numbers, while avoiding the electronic repulsions from the pyridine ring with high electron density.

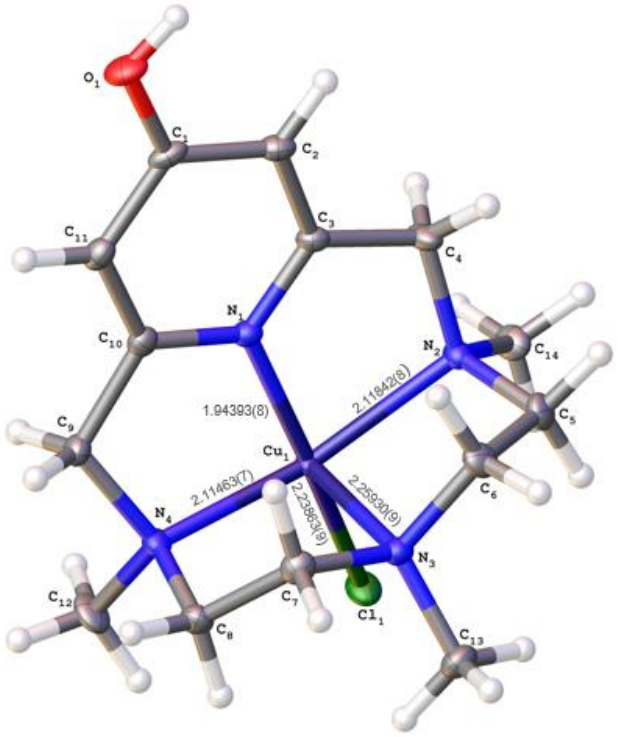

Figure 10. X-ray crystal structure of $[CuCl(\mathbf{Me_3L_2})]^{2+}$ with associated atom labels and bond distances of interest.

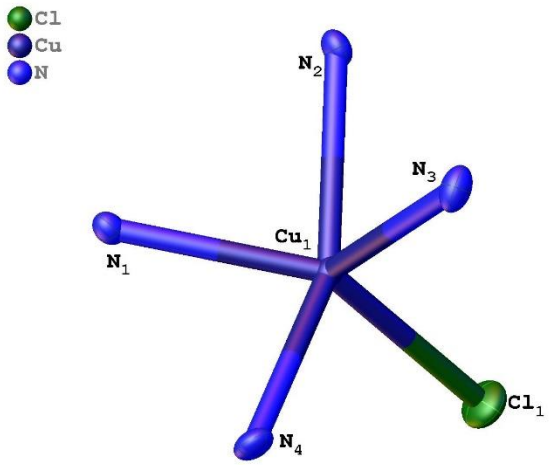

Figure 11. Representation the coordination of Cu^{II} center in a $[CuCl(\mathbf{L})]^{2+}$ unit.

Table 3. Comparison of selected bond angle/^{o} between $[CuCl(\mathbf{Me_3L_2})]^{2+}$ and $[CuCl(\mathbf{L_2})]^{2+}$.

Atom	Atom	Atom	Bond Angle/^{o}	
			$[CuCl(\mathbf{L_2})]^{2+}$	$[CuCl(\mathbf{Me_3L_2})]^{2+}$
N_1	Cu_1	N_2	81.87(6)	81.52(7)
N_2	Cu_1	N_3	84.44(7)	84.90(6)
N_3	Cu_1	N_4	84.49(7)	84.85(6)
N_4	Cu_1	N_1	81.79(6)	81.03(7)
N_1	Cu_1	N_3	98.89(6)	96.11(7)
N_4	Cu_1	N_2	158.57(6)	158.67(6)
Cl_1	Cu_1	N_1	154.20(5)	166.20(5)
Cl_1	Cu_1	N_2	100.69(5)	98.08(5)
Cl_1	Cu_1	N_3	106.91(5)	97.60(5)
Cl_1	Cu_1	N_4	100.07(5)	101.79(5)

Table 4. Comparison of selected bond length between $[CuCl(\mathbf{Me_3L_2})]^{2+}$ and $[CuCl(\mathbf{L_2})]^{2+}$.

Selected atoms	Bond length (Å)	
	$[CuCl(\mathbf{L_2})]^{2+}$	$[CuCl(\mathbf{Me_3L_2})]^{2+}$
Cu-N_1	1.93(916)	1.94(394)
Cu-N_2	2.08(216)	2.11(843)
Cu-N_3	2.17(319)	2.25(931)
Cu-N_4	2.07(916)	2.11(464)
Cu-Cl_1	2.22(69)	2.23(639)

UV-Vis Spectroscopic Analysis

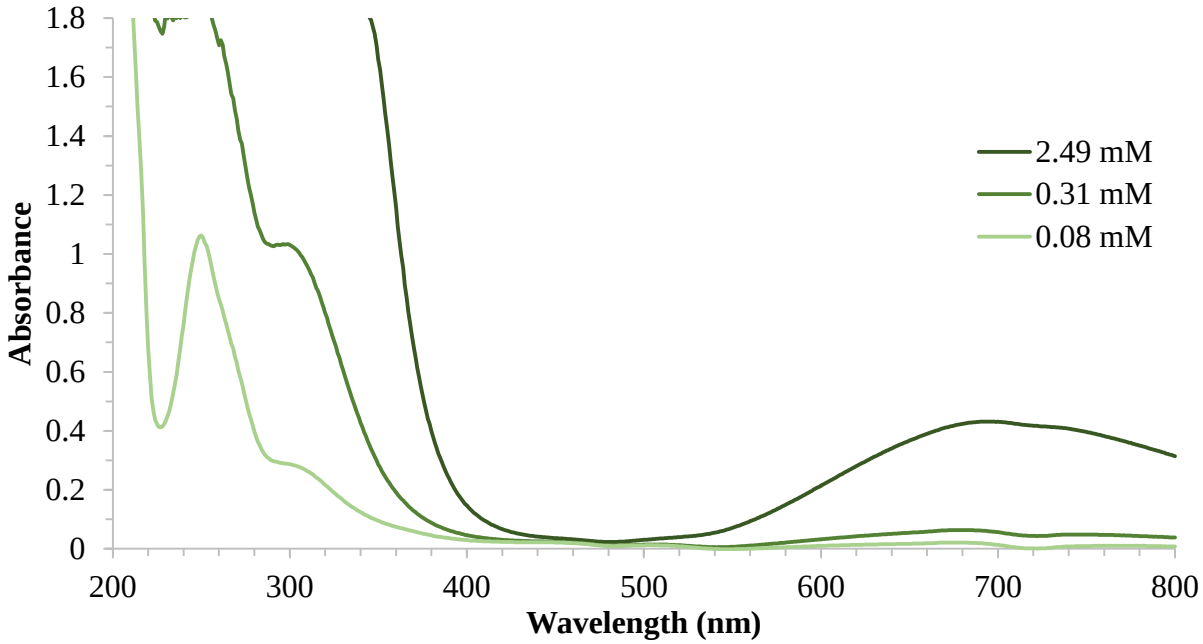

Figure 12. UV-Vis spectra of $CuCl(\mathbf{Me_3L_2})ClO_4$ solutions in water at different concentrations (2.49, 0.31 and 0.08 mM) with absorption peaks at 250 nm (9.01×10^3 $M^{-1}cm^{-1}$), 300 nm (3.19×10^3 $M^{-1}cm^{-1}$) and 700 nm (0.17×10^3 $M^{-1}cm^{-1}$).

UV-Vis spectroscopic analysis (as shown in **Figure 12**) was performed on the solution of $CuCl(\mathbf{Me_3L_2})ClO_4$ at room temperature to show $\pi \rightarrow \pi^*$ and d → d transitions from the aromatic

ring and copper (II), respectively. **Me$_3$L$_2$** contains absorbance bands at 260 nm (1.78×10^4 $M^{-1}cm^{-1}$, **Appendix**, **Figure A8**). Upon complexation with copper (II), a blue shift is observed associated with the $\pi \rightarrow \pi^*$ transition event, which is observed at 250 nm (9.01×10^3 $M^{-1}cm^{-1}$) and 300 nm (3.19×10^3 $M^{-1}cm^{-1}$). A d → d absorption band was also observed at 700 nm (0.17×10^3 $M^{-1}cm^{-1}$) for CuCl(**Me$_3$L$_2$**)ClO_4 complex. The absorption wavelengths and molar absorptivity associated with each transition event are in agreement between CuCl(**Me$_3$L$_2$**)ClO_4 and CuCl(**L$_2$**)ClO_4 complex, as illustrated in **Table 5**. This observation is within expectation as the introduced methyl groups on aliphatic amines do not have significant electronic effects on the pyridine ring. Thus, $\pi \rightarrow \pi^*$ transition within the pyridine ring is barely affected. However, the same conclusion cannot be made about the effect of introduced methyl groups on the copper (II) center, since the d-d band associated with copper (II) is usually broad. Cyclic voltammetry will be able to reveal more information about the electronic behavior of the copper center in CuCl(**Me$_3$L$_2$**)ClO_4.

Table 5. UV-Vis spectroscopic properties of CuCl[**L**]ClO_4 complexes.

Compound	**λ_{abs}, nm (molar absorptivity × 10^3 $M^{-1}cm^{-1}$)**
[Cu(**Me$_3$L$_2$**)Cl](ClO_4) (in water)	250 (9.01 ± 0.66) 300 (3.19 ± 0.01) 700 (0.17 ± 0.00)
[Cu(**L$_2$**)Cl](ClO_4) (in water)	249 (8.78) 284-330 (sh) 699 (0.107)

Cyclic Voltammetry

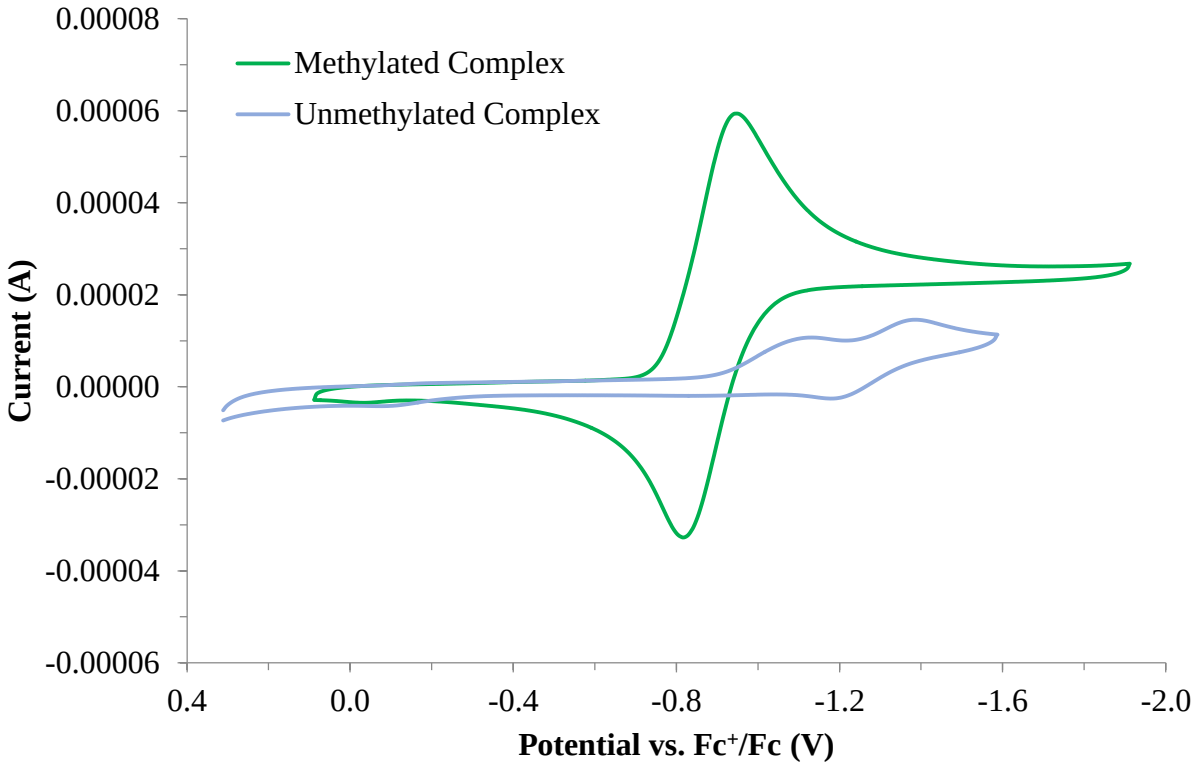

Figure 13. Cyclic voltammogram obtained for CuCl(**Me$_3$L$_2$**)ClO$_4$ 4.87 mM (green) and CuCl(**L$_2$**)ClO$_4$ 3.1 mM (blue) solution in DMF containing tetrabutylammonium tetrafluoroborate as the supporting electrolyte at a scan rate of 100 mV/s. Electrochemical study of CuCl(**L$_2$**)ClO$_4$ was previously performed by Kimberly *et al.*[16] The potential values axis have been adjusted using the half-way potential of Fc^+/Fc redox couple as reference ($E_{1/2}$ = 0.0 mV).

Electron-transfer reactions between metal centers within and between metalloprotein molecules is a subject of great interest. Cyclic voltammetry is perhaps the most versatile electroanalytical technique for the study of electroactive species. The theory of cyclic voltammetry has been extended to include electron transfer reactions which are described by the electrochemical rate (Nernst) equation.

Electrochemical experiments showed that the introduction of methyl groups in CuCl(**Me$_3$L$_2$**)ClO$_4$ complex greatly influence the redox behavior of the copper center in comparison to CuCl(**L$_2$**)ClO$_4$. A reversible redox couple was observed at $E_{1/2}$ = -882 mV (**Figure 13**), which can be assigned to the Cu^{II}/Cu^{I} redox couple of the CuCl(**Me$_3$L$_2$**)ClO$_4$ complex. The reversible redox reaction was diffusion controlled (**Appendix**, **Figure A7**). Comparison with the half-way potential of **L$_2$**Cu^{II}/**L$_2$**Cu^{I} redox cycle associated with CuCl(**L$_2$**)ClO$_4$ (-1200 mV, **Table 6**) showed that copper (II) is more easily reduced to copper (I) in presence of **Me$_3$L$_2$**.

From electrochemical characterization, it is speculative that **Me$_3$L$_2$** can show both catalytic and inhibitor activity worthy of further investigation. While the catalytic behavior of CuCl(**Me$_3$L$_2$**)ClO$_4$ complex has not yet been thoroughly studied due to the challenge in finding suitable detection method to identify possible side products and calculate yield over microscale, it is known that Cu^{I} oxidation and Cu^{II} reduction is associated with, respectively, hydrocarbon sp^3C-H hydroxylation and inhibition toward the generation of toxic reactive oxygen species *in vivo*, as previously mentioned in the introduction. CuCl(**Me$_3$L$_2$**)ClO$_4$ complex can help broaden the scope of catalyst library in an effort to mimic the hydrocarbon hydroxylation ability of cytochrome P450 enzymes.

Table 6. Half-way potential ($E_{1/2}$) values for Cu^{II}/Cu^{I} redox processes.

Compound	**$E_{1/2}$ (mV)**
CuCl(**Me$_3$L$_2$**)ClO$_4$ (in DMF)	-882
CuCl(**L$_2$**)ClO$_4$ (in DMF)	-1200

*The data reported has been normalized to the value of half-way potential for Fc/Fc^+ redox couple.

CONCLUSION AND FUTURE DIRECTIONS

In this research work, a new ligand was synthesized and could potentially enrich the library of aromatic MPAs that have been recently investigated by bioinorganic chemists. It was seen that by introducing the methyl groups on nitrogen atoms of **L_2**, the electrochemical behavior of the copper-centered complex is greatly influenced (-882 mV vs. -1200 mV), while the three-dimensional structure of the complex remains almost unchanged. This finding gives foundation to the catalytic and biological study of the complex.

The catalytic activity, based on Cu^I oxidation, of CuCl(**Me_3L_2**)ClO_4 complex was tested with the carbon-hydrogen hydroxylation of cyclohexane with a catalytic amount of hydrogen peroxide; however, the appropriate detection and analytical method toward the presence of cyclohexanol as product has not yet been discovered. Gas chromatography-mass spectroscopy (GC-MS) is currently looked into, but the proximity in both boiling point and molecular weight of cyclohexanol and cyclohexanone (an oxidative side product) proves a challenge toward this analytical method.

In addition, electrochemical study of the copper-centered complex of the ligand showed that the reduction of copper (II) to copper (I) is more favorable in presence of **Me_3L_2** compared to in presence of **L_2**. The results suggest that **Me_3L_2** can act as an inhibitor toward the Cu^I oxidation to Cu^{II} responsible for the production of reactive oxidative species in biological systems. Further biological analysis, for example by the 2-deoxyribose assay which measures the capacity of ligands to control the formation of copper-catalyzed hydroxyl radicals,[34] will help uncover the inhibitory effect of **Me_3L_2**.

APPENDIX

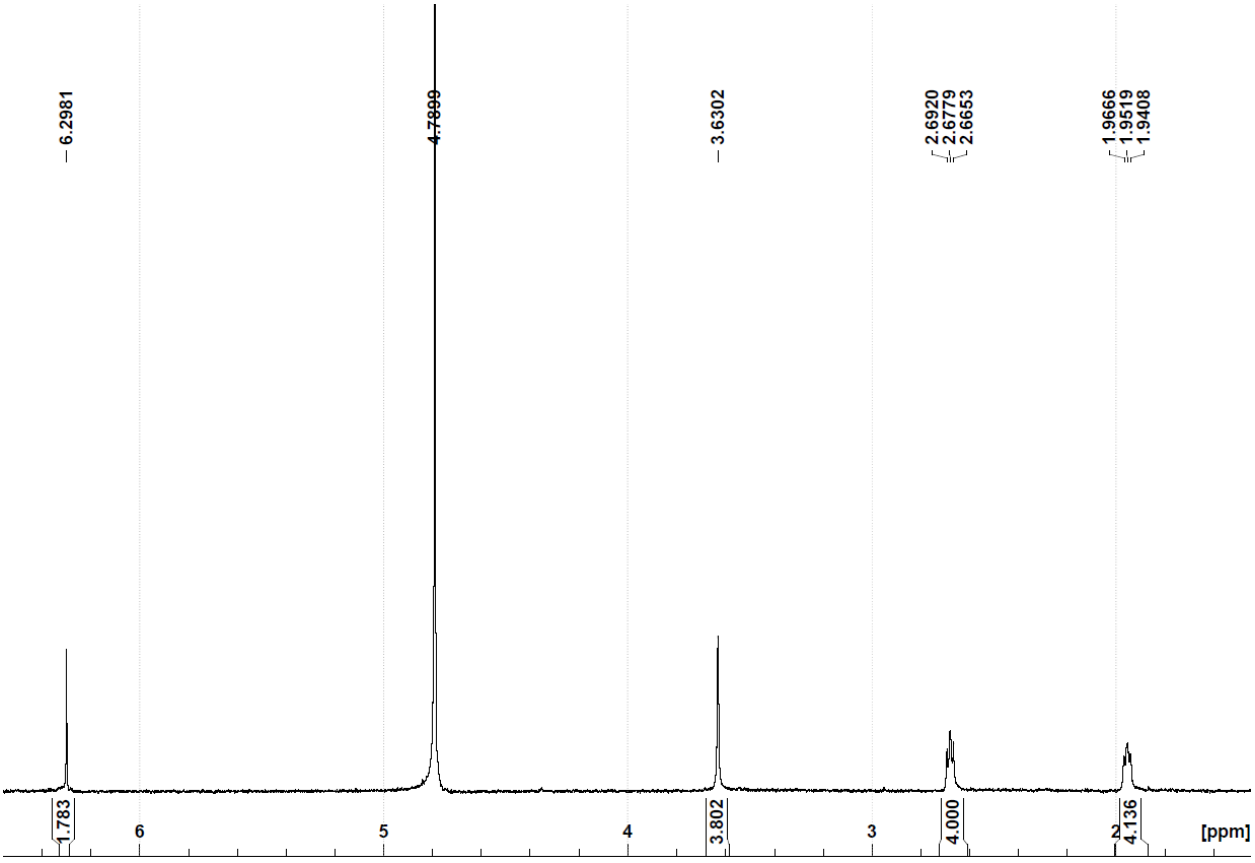

Figure A1. ^{1}H NMR spectrum of **L_2** in D_2O at pH = 14 and chemical structure of **L_2** with protons labeled from (a) to (d).

Table A1. Assigned protons to observed peaks in ^{1}H NMR spectroscopy

Observed peak (ppm)	Multiplicity	Integration	Assigned proton
6.30	Singlet	1.78	(a)
3.63	Singlet	3.80	(b)
2.68	Triplet	4.00	(c)
1.95	Triplet	4.14	(d)

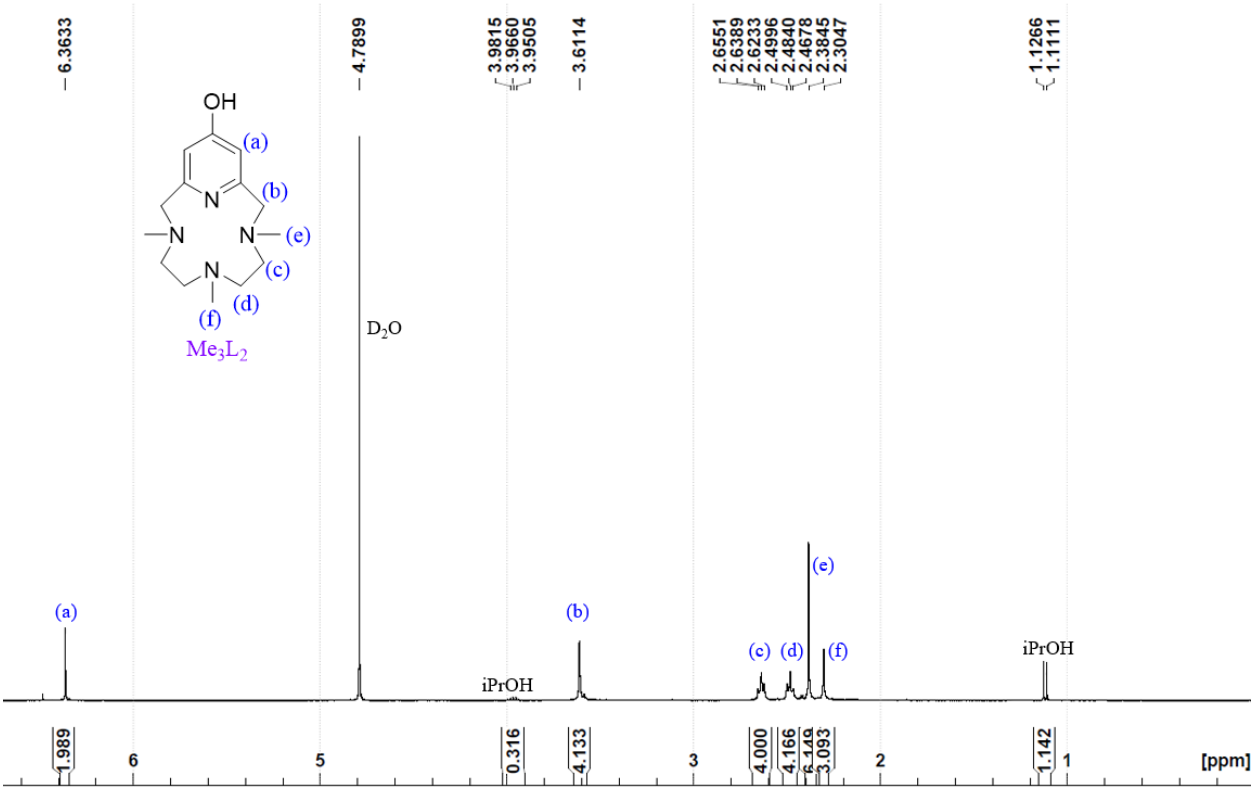

Figure A2. ^{1}H NMR spectrum of Me_3L_2 in D_2O at pH = 11.8 and chemical structure of **Me_3L_2** with protons labeled from (a) to (e).

Table A2. Assigned protons to observed peaks in ^{1}H NMR spectroscopy

Observed peak (ppm)	Multiplicity	Integration	Assigned proton
6.36	Singlet	1.99	(a)
3.61	Singlet	4.31	(b)
2.64	Triplet	4.00	(c)
2.48	Triplet	4.17	(d)
2.38	Singlet	6.33	(e)
2.30	Singlet	3.56	(f)

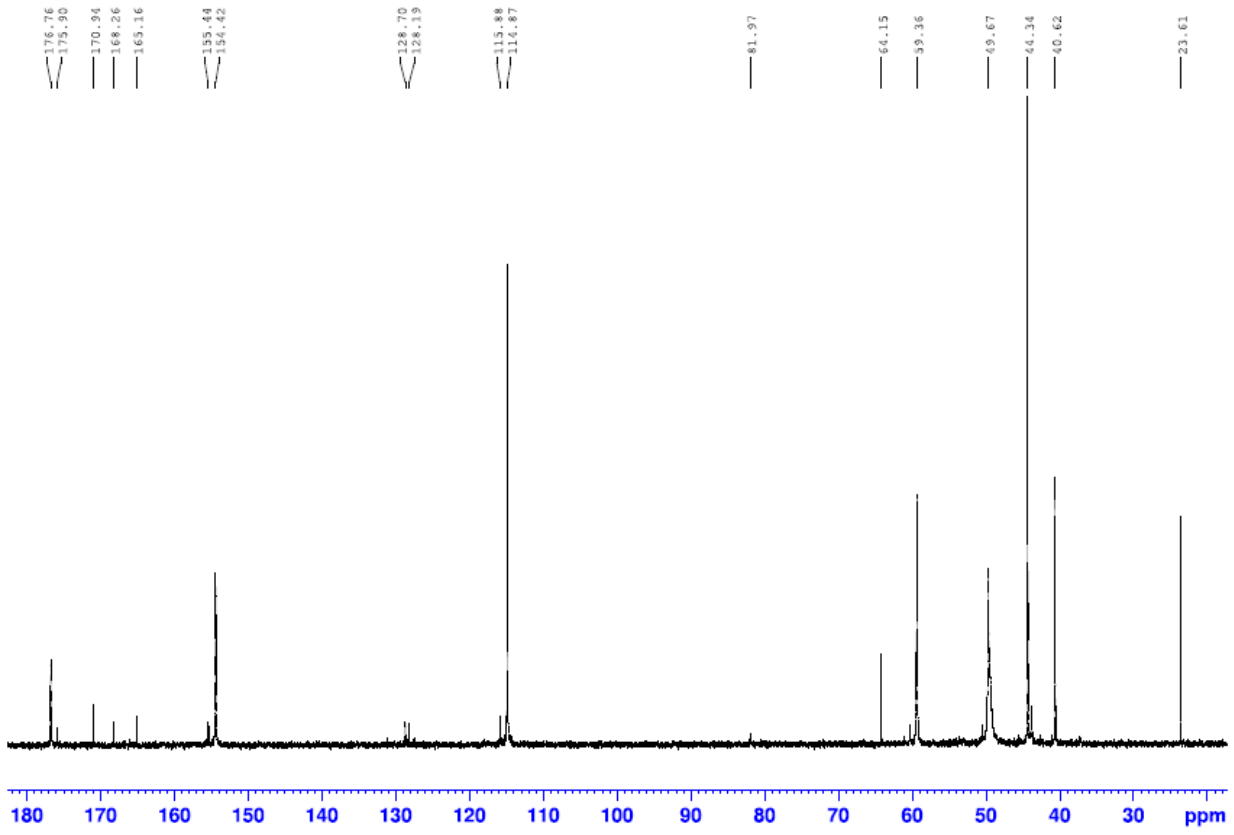

Figure A3. ^{13}C NMR spectrum of **Me$_3$L$_2$**.

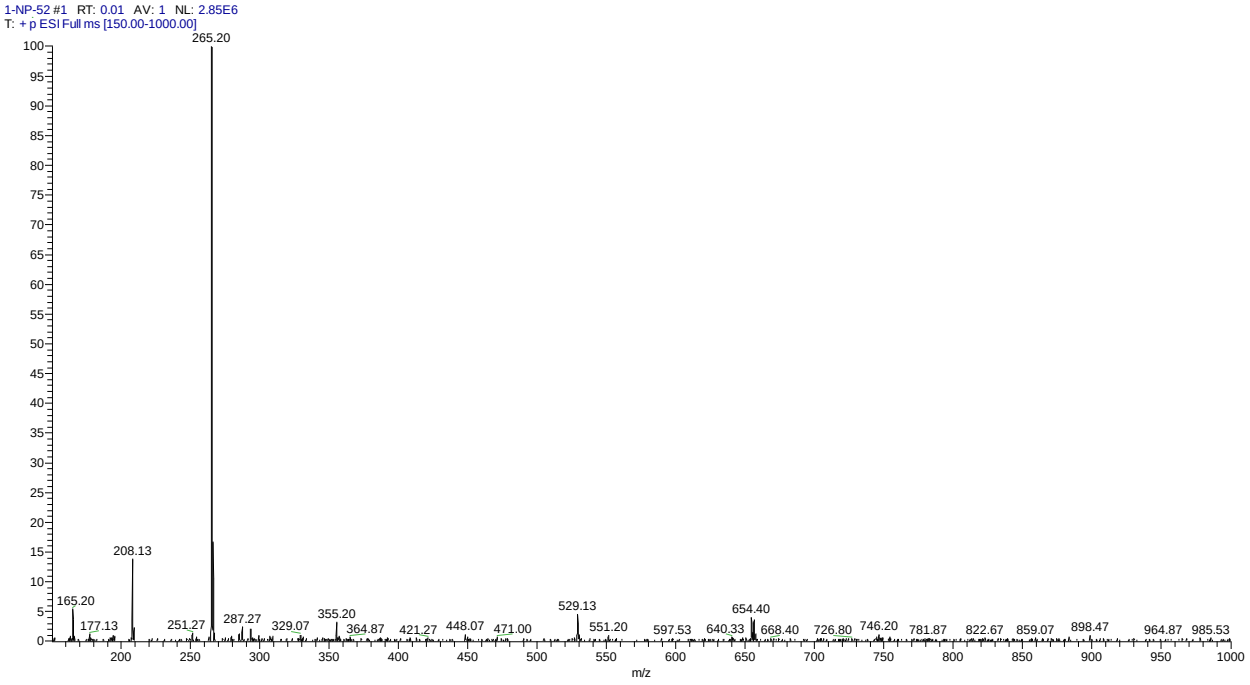

Figure A4. IT/MS spectrum of **Me$_3$L$_2$**.

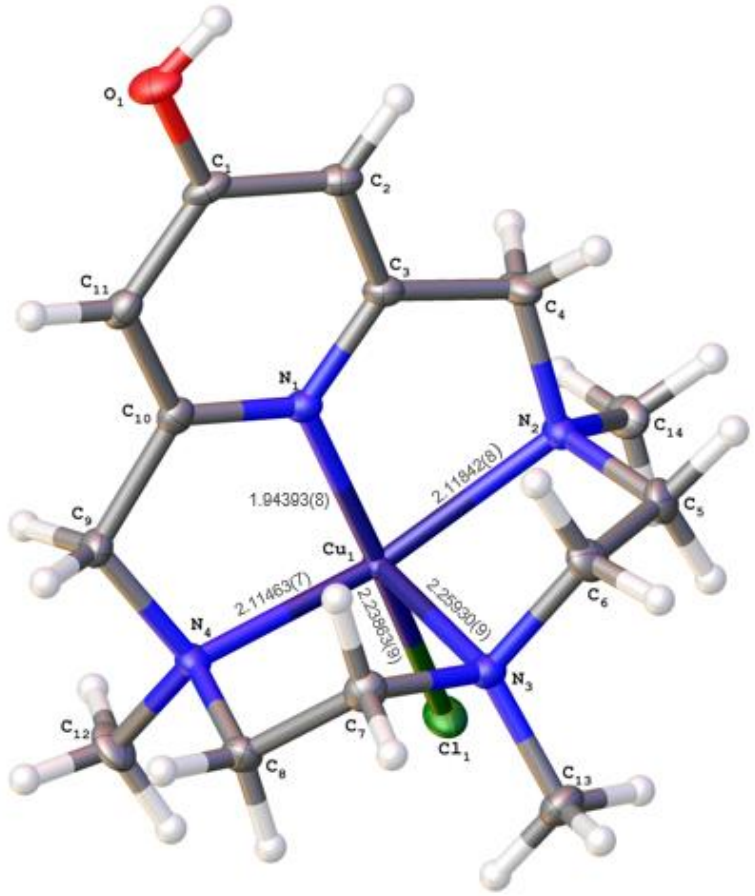

Figure A5. X-ray crystal structure of one asymmetric unit of [CuCl(**Me$_3$L$_2$**)ClO$_4$]$_2$(ClO$_4$)$_2$(H$_2$O).

Table A3. Crystal data and structure refinement for CuCl(**Me$_3$L$_2$**)ClO$_4$.

Identification code	[**Me$_3$L$_2$**]CuCl
Empirical formula	$C_{14}H_{25}Cl_2CuN_4O_{5.5}$
Formula weight	471.82
Temperature/K	107.56
Crystal system	monoclinic
Space group	C2/c
a/Å	44.632(3)
b/Å	13.5633(8)
c/Å	13.1507(7)
α/°	90

β/°	106.664(2)
γ/°	90
Volume/Å^3	7626.6(8)
Z	16
ρ_{calc}g/cm^3	1.644
μ/mm^{-1}	1.462
F(000)	3904.0
Crystal size/mm^3	0.810 × 1.150 × 1.540
Radiation	MoKα (λ = 0.71073)
2Θ range for data collection/°	5.716 to 56.786
Index ranges	-59 ≤ h ≤ 59, -18 ≤ k ≤ 18, -17 ≤ l ≤ 17
Reflections collected	160369
Independent reflections	9524 [R_{int} = 0.0361, R_{sigma} = 0.0135]
Data/restraints/parameters	9524/0/489
Goodness-of-fit on F^2	1.027
Final R indexes [I>=2σ (I)]	R_1 = 0.0331, wR_2 = 0.0814
Final R indexes [all data]	R_1 = 0.0374, wR_2 = 0.0843
Largest diff. peak/hole / e Å^{-3}	2.08/-0.79

Table A4. Bond Lengths for [**Me$_3$L$_2$**]CuCl.

Atom	Atom	Length/Å		Atom	Atom	Length/Å
Cu_1	Cl_1	2.2386(5)		N_3	C_{13}	1.471(3)
Cu_1	N_1	1.9439(16)		N_4	C_9	1.495(3)

Cu_1	N_3	2.2593(17)		N_4	C_8	1.496(3)
Cu_1	N_4	2.1146(17)		N_4	C_{12}	1.481(3)
Cu_1	N_2	2.1184(17)		N_6	C_{26}	1.486(2)
Cu_2	Cl_2	2.2964(5)		N_6	C_{19}	1.507(3)
Cu_2	N_8	2.0932(16)		N_6	C_{18}	1.488(3)
Cu_2	N_5	1.9499(16)		N_7	C_{27}	1.468(3)
Cu_2	N_6	2.1025(17)		N_7	C_{21}	1.501(3)
Cu_2	N_7	2.1000(17)		N_7	C_{20}	1.475(3)
Cl_3	O_{10}	1.4549(16)		N_2	C_4	1.486(3)
Cl_3	O_8	1.4335(18)		N_2	C_5	1.491(3)
Cl_3	O_7	1.424(2)		**N_2**	**C_{14}**	1.481(3)
Cl_3	O_9	1.426(2)		C_{24}	C_{25}	1.377(3)
Cl_4	O_6	1.420(2)		C_{24}	C_{23}	1.504(3)
Cl_4	O_5	1.4285(19)		C_{16}	C_{17}	1.375(3)
Cl_4	O_3	1.451(2)		C_{16}	C_{15}	1.397(3)
Cl_4	O_4	1.409(2)		C_{25}	C_{15}	1.398(3)
O_2	C_{15}	1.339(2)		C_{17}	C_{18}	1.499(3)
O_1	C_1	1.347(2)		C_3	C_4	1.500(3)
N_8	C_{28}	1.479(2)		C_3	C_2	1.378(3)
N_8	C_{23}	1.491(2)		C_{10}	C_9	1.499(3)
N_8	C_{22}	1.486(2)		C_{10}	C_{11}	1.380(3)
N_5	C_{24}	1.341(2)		C_{11}	C_1	1.395(3)
N_5	C_{17}	1.340(2)		C_1	C_2	1.394(3)
N_1	C_3	1.339(2)		C_5	C_6	1.527(3)
N_1	C_{10}	1.339(3)		C_8	C_7	1.524(3)
N_3	C_6	1.472(3)		C_{22}	C_{21}	1.497(3)
N_3	C_7	1.471(3)		C_{19}	C_{20}	1.518(3)

Table A5. Bond Angles for Me3L2Cu_081018_0m_a.

Atom	Atom	Atom	Angle/°		Atom	Atom	Atom	Angle/°
Cl_1	Cu_1	N_3	97.60(5)		C_{12}	N_4	C_9	107.84(16)
N_1	Cu_1	Cl_1	166.20(5)		C_{12}	N_4	C_8	109.21(17)
N_1	Cu_1	N_3	96.11(7)		C_{26}	N_6	Cu_2	115.62(13)
N_1	Cu_1	N_4	81.03(7)		C_{26}	N_6	C_{19}	108.60(16)
N_1	Cu_1	N_2	81.52(7)		C_{26}	N_6	C_{18}	107.93(16)
N_4	Cu_1	Cl_1	101.79(5)		C_{19}	N_6	Cu_2	105.10(12)
N_4	Cu_1	N_3	84.85(6)		C_{18}	N_6	Cu_2	107.48(12)
N_4	Cu_1	N_2	158.67(6)		C_{18}	N_6	C_{19}	112.20(17)
N_2	Cu_1	Cl_1	98.08(5)		C_{27}	N_7	Cu_2	118.34(13)
N_2	Cu_1	N_3	84.90(6)		C_{27}	N_7	C_{21}	108.36(17)
N_8	Cu_2	Cl_2	102.89(5)		C_{27}	N_7	C_{20}	113.09(17)
N_8	Cu_2	N_6	154.04(6)		C_{21}	N_7	Cu_2	106.29(12)
N_8	Cu_2	N_7	86.24(6)		C_{20}	N_7	Cu_2	98.86(12)
N_5	Cu_2	Cl_2	130.97(5)		C_{20}	N_7	C_{21}	111.52(16)
N_5	Cu_2	N_8	80.61(6)		C_4	N_2	Cu_1	108.89(12)
N_5	Cu_2	N_6	81.85(6)		C_4	N_2	C_5	111.13(16)
N_5	Cu_2	N_7	118.51(7)		C_5	N_2	Cu_1	104.35(12)
N_6	Cu_2	Cl_2	103.05(5)		C_{14}	N_2	Cu_1	114.52(13)
N_7	Cu_2	Cl_2	110.53(5)		C_{14}	N_2	C_4	108.07(16)
N_7	Cu_2	N_6	85.48(7)		C_{14}	N_2	C_5	109.89(16)
O_8	Cl_3	O_{10}	108.81(11)		N_5	C_{24}	C_{25}	121.84(17)
O_7	Cl_3	O_{10}	108.14(12)		N_5	C_{24}	C_{23}	112.76(16)
O_7	Cl_3	O_8	110.24(13)		C_{25}	C_{24}	C_{23}	125.38(17)
O_7	Cl_3	O_9	110.14(16)		C_{17}	C_{16}	C_{15}	118.45(18)
O_9	Cl_3	O_{10}	109.27(12)		C_{24}	C_{25}	C_{15}	117.95(17)

O_9	Cl_3	O_8	110.19(13)		N_5	C_{17}	C_{16}	121.52(17)
O_6	Cl_4	O_5	111.01(13)		N_5	C_{17}	C_{18}	113.39(17)
O_6	Cl_4	O_3	105.45(16)		C_{16}	C_{17}	C_{18}	124.98(18)
O_5	Cl_4	O_3	107.52(14)		N_1	C_3	C_4	114.93(17)
O_4	Cl_4	O_6	110.65(16)		N_1	C_3	C_2	122.17(19)
O_4	Cl_4	O_5	112.48(14)		C_2	C_3	C_4	122.81(18)
O_4	Cl_4	O_3	109.44(19)		N_1	C_{10}	C_9	114.18(17)
C_{28}	N_8	Cu_2	117.50(13)		N_1	C_{10}	C_{11}	121.43(19)
C_{28}	N_8	C_{23}	108.87(15)		C_{11}	C_{10}	C_9	124.32(18)
C_{28}	N_8	C_{22}	111.42(16)		N_8	C_{23}	C_{24}	109.34(15)
C_{23}	N_8	Cu_2	107.97(11)		N_4	C_9	C_{10}	111.42(16)
C_{22}	N_8	Cu_2	101.72(12)		C_{10}	C_{11}	C_1	118.47(19)
C_{22}	N_8	C_{23}	108.95(16)		O_2	C_{15}	C_{16}	117.38(18)
C_{24}	N_5	Cu_2	119.50(13)		O_2	C_{15}	C_{25}	122.84(18)
C_{17}	N_5	Cu_2	118.63(13)		C_{16}	C_{15}	C_{25}	119.77(17)
C_{17}	N_5	C_{24}	120.42(16)		O_1	C_1	C_{11}	118.35(19)
C_3	N_1	Cu_1	119.51(13)		O_1	C_1	C_2	121.80(19)
C_3	N_1	C_{10}	120.21(17)		C_2	C_1	C_{11}	119.86(18)
C_{10}	N_1	Cu_1	120.16(14)		N_2	C_4	C_3	111.90(16)
C_6	N_3	Cu_1	100.64(12)		N_2	C_5	C_6	112.61(17)
C_7	N_3	Cu_1	99.86(12)		N_4	C_8	C_7	112.48(16)
C_7	N_3	C_6	115.19(16)		N_3	C_6	C_5	109.14(17)
C_7	N_3	C_{13}	111.01(17)		N_8	C_{22}	C_{21}	111.83(17)
C_{13}	N_3	Cu_1	118.96(13)		N_6	C_{19}	C_{20}	113.23(17)
C_{13}	N_3	C_6	110.71(16)		C_3	C_2	C_1	117.87(19)
C_9	N_4	Cu_1	108.51(12)		N_6	C_{18}	C_{17}	111.28(16)
C_9	N_4	C_8	111.09(16)		N_3	C_7	C_8	109.90(17)

C_8	N_4	Cu_1	105.30(12)		C_{22}	C_{21}	N_7	111.46(17)
C_{12}	N_4	Cu_1	114.90(13)		N_7	C_{20}	C_{19}	110.75(18)

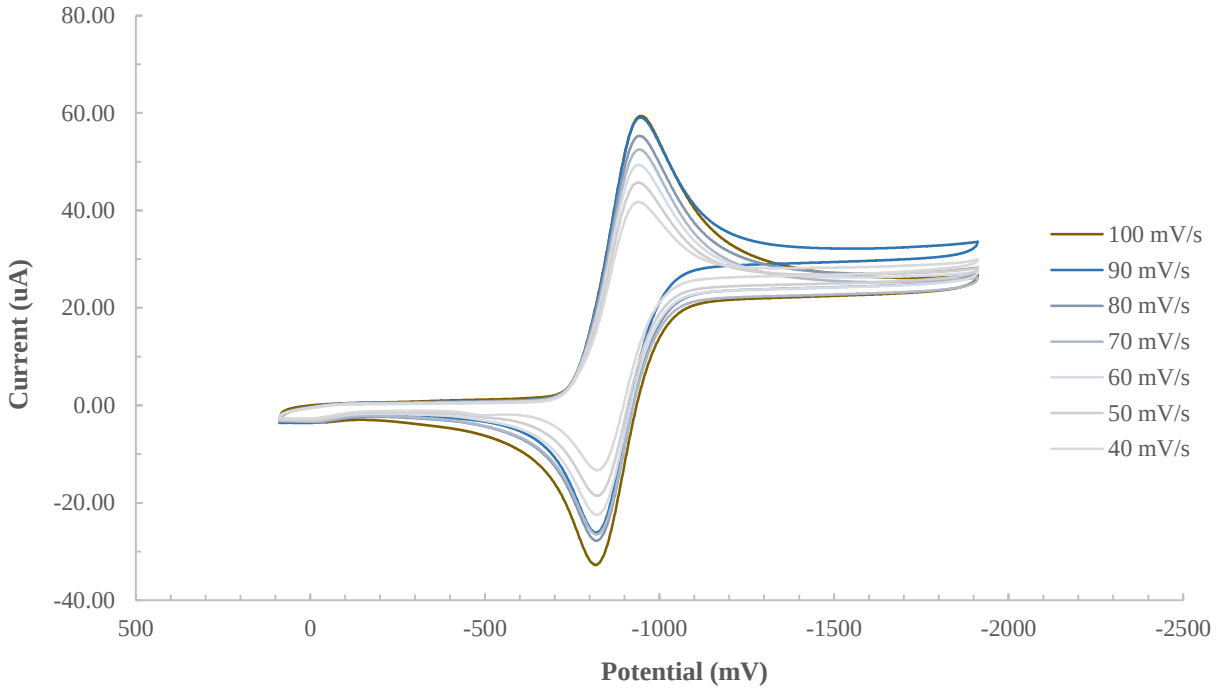

Figure A6. Cyclic voltammogram obtained for [Cu(**Me$_3$L$_2$**)Cl](ClO$_4$) 4.87 mM solution in DMF containing tetrabutylammonium tetrafluoroborate as the supporting electrolyte at different scan rates of 100, 90, 80, 70, 60, 50, 40 mV/s. The potential values axis have been adjusted using the half-way potential of Fc(III)/Fc(II) redox couple as reference ($E_{1/2\ Fc(III)/Fc(II)}$ = 0 mV)

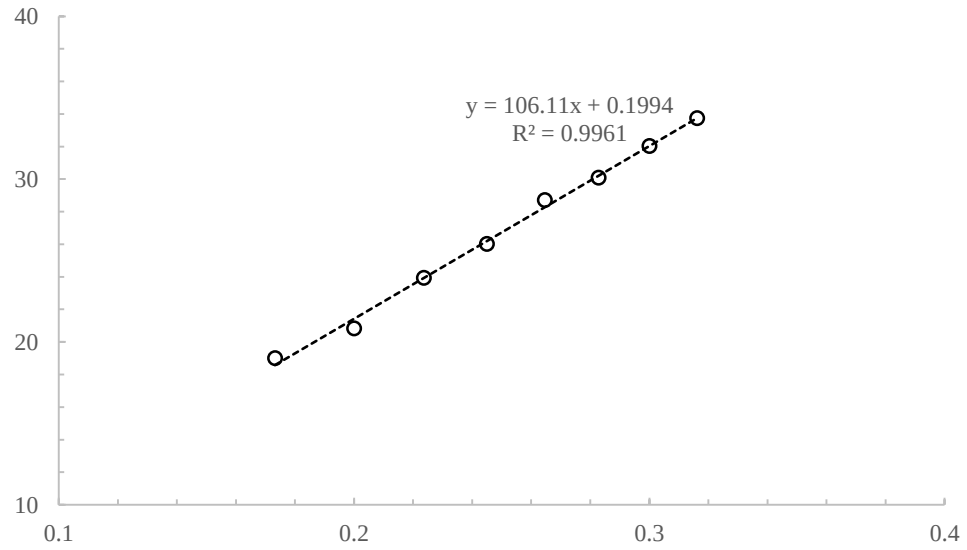

Figure A7. Plot for the cathodic peak current as a function of the square root of the scan rate for [Cu(**Me$_3$L$_2$**)Cl](ClO$_4$) 4.87 mM solution in DMF containing tetrabutylammonium tetrafluoroborate as the supporting electrolyte at different scan rates of 100, 90, 80, 70, 60, 50, 40 mV/s. Linearity of the function is the proof for diffusion controlled experiment.

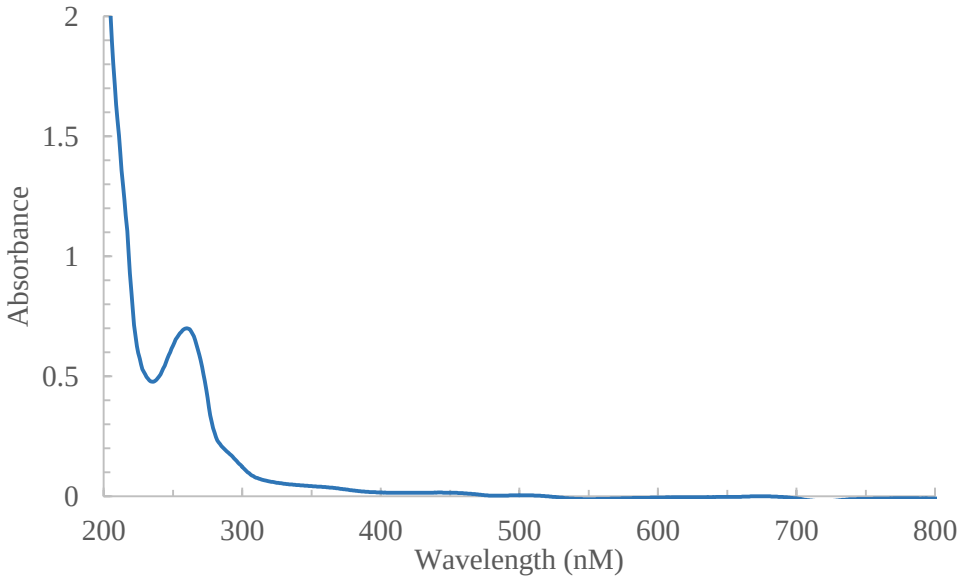

Figure A8. UV-Vis spectroscopy of 0.6 mM **Me$_3$L$_2$** in H_2O. Molar absorptivity of the solution is $(17.76 \pm 0.02) \times 10^3$ $M^{-1}cm^{-1}$.

REFERENCES

1. Anastas, P. T.; Warner, J. C., *Green Chemistry: Theory and Practice*. Oxford University Press: New York, 1998.

2. Kolb, D., Catalysis. *Journal of Chemical Education* **1979,** *56* (11), 743.

3. Rothlisberger, D.; Khersonsky, O.; Wollacott, A. M.; Jiang, L.; DeChancie, J.; Betker, J.; Gallaher, J. L.; Althoff, E. A.; Zanghellini, A.; Dym, O.; Albeck, S.; Houk, K. N.; Tawfik, D. S.; Baker, D., Kemp elimination catalysts by computational enzyme design. *Nature* **2008,** *453* (7192), 190-5.

4. Parisi, E., METALLOPROTEINS: CHROMATOGRAPHY. In *Encyclopedia of Separation Science*, Wilson, I. D., Ed. Academic Press: Oxford, 2000; pp 3380-3386.

5. Lehninger, A. L.; Nelson, D. L.; Cox, M. M., *Lehninger Principles of Biochemistry*. W.H. Freeman: New York, 2008.

6. Lippard, S. J.; Berg, J. M., *Principles of Bioinorganic Chemistry*. Panima Publishing Corporation: New Delhi, 2005.

7. Fricker, S. P., Metal Based Drugs: From Serendipity to Design. *Dalton Trans* **2007,** (43), 4903-17.

8. Mjos, K. D.; Orvig, C., Metallodrugs in Medicinal Inorganic Chemistry. *Chem Rev* **2014,** *114* (8), 4540-63.

9. Bruijnincx, P. C.; Sadler, P. J., New Trends for Metal Complexes with Anticancer Activity. *Curr Opin Chem Biol* **2008,** *12* (2), 197-206.

10. Le Fur, M.; Molnar, E.; Beyler, M.; Fougere, O.; Esteban-Gomez, D.; Rousseaux, O.; Tripier, R.; Tircso, G.; Platas-Iglesias, C., Expanding the Family of Pyclen-Based Ligands

Bearing Pendant Picolinate Arms for Lanthanide Complexation. *Inorg Chem* **2018,** *57* (12), 6932-6945.

11. Yu, X.; Zhang, J., Macrocyclic Polyamines : Synthesis and Applications. **2018**.

12. Pirovano, V.; Brambilla, E.; Tseberlidis, G., [Copper(I)(Pyridine-Containing Ligand)] Catalyzed Regio- and Steroselective Synthesis of 2-Vinylcyclopropa[b]indolines from 2-Vinylindoles. *Org Lett* **2018,** *20* (2), 405-408.

13. Viswanathan, S.; Kovacs, Z.; Green, K. N.; Ratnakar, S. J.; Sherry, A. D., Alternatives to Gadolinium-Based Metal Chelates for Magnetic Resonance Imaging. *Chem. Rev.* **2010,** *110* (5), 2960-3018.

14. Le Fur, M.; Beyler, M.; Molnár, E.; Fougère, O.; Esteban-Gómez, D.; Tircsó, G.; Platas-Iglesias, C.; Lepareur, N.; Rousseaux, O.; Tripier, R., Stable and Inert Yttrium(III) Complexes with Pyclen-Based Ligands Bearing Pendant Picolinate Arms: Toward New Pharmaceuticals for β-Radiotherapy. *Inorganic Chemistry* **2018,** *57* (4), 2051-2063.

15. Lincoln, K. M.; Gonzalez, P.; Richardson, T. E.; Julovich, D. A.; Saunders, R.; Simpkins, J. W.; Green, K. N., A potent antioxidant small molecule aimed at targeting metal-based oxidative stress in neurodegenerative disorders. *Chem Commun (Camb)* **2013,** *49* (26), 2712-4.

16. Lincoln, K. M.; Offutt, M. E.; Hayden, T. D.; Saunders, R. E.; Green, K. N., Structural, spectral, and electrochemical properties of nickel(II), copper(II), and zinc(II) complexes containing 12-membered pyridine- and pyridol-based tetra-aza macrocycles. *Inorg Chem* **2014,** *53* (3), 1406-16.

17. Serrano-Plana, J.; Aguinaco, A.; Belda, R.; Garcia-Espana, E.; Basallote, M. G.; Company, A.; Costas, M., Exceedingly Fast Oxygen Atom Transfer to Olefins via a Catalytically Competent Nonheme Iron Species. *Angew Chem Int Ed Engl* **2016,** *55* (21), 6310-4.

18. Shin, B.; Sutherlin, K. D.; Ohta, T.; Ogura, T.; Solomon, E. I.; Cho, J., Reactivity of a Cobalt(III)-Hydroperoxo Complex in Electrophilic Reactions. *Inorg Chem* **2016,** *55* (23), 12391-12399.

19. Name-Reaction Eischweiler-Clarke Reaction. https://www.name-reaction.com/eschweiler-clarke-reaction.

20. Garcia-Bosch, I., Copper-Catalyzed Oxidation of Alkanes under Mild Conditions. *Synlett* **2017,** *28* (11), 1237-1243.

21. Guilloreau, L.; Combalbert, S.; Sournia-Saquet, A.; Mazarguil, H.; Faller, P., Redox Chemistry of Copper–Amyloid-β: The Generation of Hydroxyl Radical in the Presence of Ascorbate is Linked to Redox-Potentials and Aggregation State. *ChemBioChem* **2007,** *8* (11), 1317-1325.

22. Bush, A. I., The metallobiology of Alzheimer's disease. *Trends in Neurosciences* **2003,** *26* (4), 207-214.

23. Gaggelli, E.; Kozlowski, H.; Valensin, D.; Valensin, G., Copper Homeostasis and Neurodegenerative Disorders (Alzheimer's, Prion, and Parkinson's Diseases and Amyotrophic Lateral Sclerosis). *Chemical Reviews* **2006,** *106* (6), 1995-2044.

24. Jiang, D.; Zhang, L.; Grant, G. P. G.; Dudzik, C. G.; Chen, S.; Patel, S.; Hao, Y.; Millhauser, G. L.; Zhou, F., The elevated copper binding strength of amyloid-β aggregates allows the sequestration of copper from albumin: a pathway to accumulation of copper in senile plaques. *Biochemistry* **2013,** *52* (3), 547-556.

25. Lincoln, K. M.; Richardson, T. E.; Rutter, L.; Gonzalez, P.; Simpkins, J. W.; Green, K. N., An N-Heterocyclic Amine Chelate Capable of Antioxidant Capacity and Amyloid Disaggregation. *ACS Chemical Neuroscience* **2012,** *3* (11), 919-927.

26. Fulmer, G. R.; Miller, A. J. M.; Sherden, N. H.; Gottlieb, H. E.; Nudelman, A.; Stoltz, B. M.; Bercaw, J. E.; Goldberg, K. I., NMR Chemical Shifts of Trace Impurities: Common Laboratory Solvents, Organics, and Gases in Deuterated Solvents Relevant to the Organometallic Chemist. *Organometallics* **2010,** *29* (9), 2176-2179.

27. Bruker AXS Inc. *APEX-2*, Bruker AXS Inc.,: Madison, WI, 2014.

28. Bruker AXS Inc. *APEX-3*, Version 1; Bruker AXS Inc.: Madison, WI, 2016.

29. Bruker AXS Inc. *SAINT*, Bruker AXS Inc.: Madison, WI, 2012.

30. Krause, L.; Herbst-Irmer, R.; Sheldrick, G. M.; Stalke, D., *J. Appl. Crystallogr.* **2015,** *48*.

31. Sheldrick, G. M. *ShelXS*, Version 2013/1; Georg-August-Universität Göttingen: Göttingen, Germany, 2013.

32. Sheldrick, G., Crystal Structure Refinement with Shelxl. *Acta Crystallographica Section C* **2015,** *71* (1), 3-8.

33. Dolomanov, O. V.; Bourhis, L. J.; Gildea, R. J.; Howard, J. A. K.; Puschmann, H., Olex2: A Complete Structure Solution, Refinement and Analysis Program. *Journal of Applied Crystallography* **2009,** *42* (2), 339-341.

34. Derrick, J. S.; Kerr, R. A.; Korshavn, K. J.; McLane, M. J.; Kang, J.; Nam, E.; Ramamoorthy, A.; Ruotolo, B. T.; Lim, M. H., Importance of the Dimethylamino Functionality on a Multifunctional Framework for Regulating Metals, Amyloid-β, and Oxidative Stress in Alzheimer's Disease. *Inorganic Chemistry* **2016,** *55* (10), 5000-5013.